
When Graph Language Models Go Beyond Memorization

Masatsugu Yamada
National Institute of Informatics
Tokyo, Japan
masatsugu-yamada@nii.ac.jp

Mahito Sugiyama
National Institute of Informatics, Tokyo, Japan
SOKENDAI, Kanagawa, Japan
mahito@nii.ac.jp

Abstract

It remains unclear whether graph language models learn structural regularities or merely memorize training graphs; this cannot be resolved by current aggregate fidelity metrics alone. We develop a calibrated diagnostic protocol that combines frequent subgraph mining, a graph-level bootstrap baseline, and three-level frequency stratification to disentangle memorization from structural alignment. Using this framework, we show that graph language models can acquire structural regularities beyond memorization at scale, primarily in the high-frequency regime. This is supported by the following empirical evidence: On five TU benchmarks, LLaMA-style graph language models reach high subgraph-rank correlation, yet their alignment is matched or exceeded by the memorization bootstrap in most cases. At small scale, under our bootstrap diagnostic, fidelity is largely indistinguishable from verbatim recall. In contrast, at large scale with 3.75M graphs, verbatim memorization drops sharply while rank correlation remains near ceiling. Crucially, in a separate fixed-subsample analysis, frequent subgraph mining restricted to the novel-only subset closely tracks the corresponding all-generation Spearman correlation, providing evidence that the alignment is not driven solely by verbatim recall. Across all scales, high-frequency patterns are well reproduced, while rare patterns remain poorly covered, and this deficit narrows only marginally as capacity increases. We observe the same scale-dependent crossover under two distinct graph serializations (canonical DFS code and action sequences), providing evidence of robustness in our analysis.

1 Introduction

Graph generation is a fundamental problem in machine learning with applications across drug discovery, material design, and social network analysis [You et al., 2018b, Li et al., 2018, Simonovsky and Komodakis, 2018, Vignac et al., 2023, Jo et al., 2022]. A growing line of work serializes graphs into token sequences and trains *graph language models*, LLM-style autoregressive decoders, to generate them, reporting strong fidelity on standard benchmarks [Goyal et al., 2020, Bagal et al., 2022, Chen et al., 2025]. Whether these models fundamentally learn structural regularities of graphs, or merely *memorize* training data and emit graphs from a near-empirical distribution, remains an open question that current aggregate fidelity metrics (degree/clustering/orbit MMD, GIN-based MMD/FID) cannot settle [You et al., 2018b, Thompson et al., 2022]: as we formalize in Corollary 3, agreement on any single bounded subgraph statistic is consistent with both regimes.

In this paper, we address this issue with a *calibrated diagnostic protocol* that focuses on *subgraph* statistics in graph databases. This protocol combines frequent subgraph mining (gSpan) Yan and Han [2002], a graph-level bootstrap baseline that resamples directly from the training corpus, and three levels of subgraph frequency stratification, Head, Torso, and Tail, of the support distribution. The bootstrap supplies the missing reference: a model is taken to go beyond memorization only

when its support statistics depart from the distribution induced by resampling training graphs, with frequency stratification then exposing where the gap concentrates.

We apply this protocol to investigate a core hypothesis: can graph language models act as *implicit neural graph miners*? While classical algorithms such as gSpan explicitly search combinatorial spaces to extract frequent subgraphs, autoregressive modeling of graph serializations may allow LLMs to internalize these same structural regularities implicitly without ever performing explicit pattern enumeration. Whether such implicit mining is possible, and, if so, to what extent, or instead confounded by verbatim recall of training graphs, is the central question that our calibrated protocol is designed to answer.

The key idea is to disentangle *implicit structural learning* from *memorization-driven alignment* along two axes simultaneously: a *memorization* axis (verbatim recall vs. novel generation) and an *alignment* axis (distributional fidelity to training subgraph statistics). The bootstrap baseline serves as the critical reference that makes this disentanglement operational. Furthermore, crossing these axes with pattern frequency stratification allows us to ask *where* across the support distribution this implicit mining succeeds or fails—a question that aggregate metrics, by construction, cannot pose.

Our contributions are summarized as follows:

- **Calibrated diagnostic protocol.** We introduce an evaluation protocol combining frequent subgraph mining with a memorization bootstrap. This protocol overcomes the limitations of aggregate fidelity metrics by disentangling true structural learning from training data memorization across different subgraph frequencies (§3, §4).
- **Scale-dependent structural learning.** We reveal that graph language models undergo a phase transition depending on scale. While models on small datasets operate in a *memorization-dominated* regime, models trained at scale enter a *decoupled* regime, successfully preserving subgraph statistics even for novel, unmemorized graphs (§6).
- **Persistent rare-pattern deficit.** Robust across different graph serializations and model capacities, our stratified diagnostic exposes a fundamental limitation: while models capture frequent substructures well, they consistently fail to learn the distribution of rare (Tail) patterns. This highlights a critical gap in current autoregressive graph generation (§6).

2 Related Work

Graph generation. Autoregressive generators produce graphs sequentially: GraphRNN [You et al., 2018b] produces adjacency rows via an RNN, GraphGen [Goyal et al., 2020] operates on minimum DFS codes, DGMG [Li et al., 2018] uses a node/edge decision process, and recent transformer-based serialized generators such as AutoGraph [Chen et al., 2025] decode graphs from a flattened token stream. Diffusion (DiGress [Vignac et al., 2023], GDSS [Jo et al., 2022], EDP-GNN [Niu et al., 2020]), VAE (GraphVAE [Simonovsky and Komodakis, 2018]), and molecular generators (GCPN [You et al., 2018a], GraphAF [Shi et al., 2020]) provide non-autoregressive alternatives; we use DiGress as our same-corpus diffusion comparator because it is a recent labeled-graph diffusion model with public training code that scales to both TU and PCQM4Mv2 under our pipeline. GraphGPT [Zhao et al., 2024] is a self-supervised graph foundation model for representation learning rather than generation. Our work is closest to GraphGen in using DFS codes, but we employ Transformer LLMs and focus on evaluation methodology rather than architecture.

Graph language models. We use *graph language models* for LLM-style autoregressive decoders trained on serialized graphs—the family our diagnostic targets. Existing instances include GraphGen [Goyal et al., 2020] (RNN over DFS codes), MolGPT [Bagal et al., 2022] (SMILES-based molecular generation), AutoGraph [Chen et al., 2025] (Transformer over flattened token streams), and the GraphGPT line [Zhao et al., 2024] (graph foundation models for representation, not generation). Adjacent work targets reasoning over text-encoded graphs [Fatemi et al., 2024, Sanford et al., 2024] or molecular property metrics (validity / novelty / drug-likeness). None of these lines probes whether the generated set reproduces local *subgraph* statistics of the training distribution at the pattern level, nor calibrates such alignment against a memorization reference. We characterize graph language models along these axes.

Memorization-aware evaluation and subgraph mining. Memorization has been extensively analyzed in language models [Carlini et al., 2021, 2023] and image diffusion [Somepalli et al., 2023]: larger models memorize more [Carlini et al., 2023], repeats concentrate memorization [Carlini et al., 2023], and training data can be extracted [Carlini et al., 2021]. These lines, however, contribute *detectors* of verbatim training examples; none provides a distributional reference against which aggregate fidelity metrics can be calibrated. The graph-generation literature is even sparser in this regard, with prior memorization analysis limited to whole-graph novelty rates [You et al., 2018b]. We close this gap on the substructure side, re-purposing gSpan [Yan and Han, 2002], which enumerates all frequent connected subgraph patterns via a canonical DFS code form with a minimum-support threshold, as the evaluation backbone. We provide the first label-aware subgraph-statistic evaluation calibrated against a graph-level memorization bootstrap.

3 A Distributional View of Sequence-Based Graph Generation

We frame sequence-based graph generation through the pushforward of a graph distribution along a serialization map. This view yields two elementary propositions that show why high distributional alignment in the sequence space, and even in subgraph statistics derived from graphs, can be confounded with memorization, motivating the calibrated protocol of §4.

Notation. Let \mathcal{G} be a space of (vertex- and edge-labeled) graphs, \mathcal{X} a space of token sequences, and $\bar{\mathcal{G}} = \mathcal{G} \cup \{\perp\}$ the graph space augmented with a sink state for malformed parses. A serialization map $\phi : \mathcal{G} \rightarrow \mathcal{X}$ (canonical DFS code, DGMG action sequence, etc.) and a measurable recovery map $\psi : \mathcal{X} \rightarrow \bar{\mathcal{G}}$ satisfy $\psi(\phi(G)) = G$. Let P_G be the true graph distribution. We denote by $P_X = \phi_{\#}P_G$ its pushforward measure along ϕ ; intuitively, P_X is the distribution of the serialized sequences $\phi(G)$ when $G \sim P_G$ (formally, $P_X(A) = P_G(\phi^{-1}(A))$ for any measurable set $A \subseteq \mathcal{X}$). Similarly, a generative model defines a sequence distribution Q_X , which induces a graph distribution $Q_G = \psi_{\#}Q_X$ on $\bar{\mathcal{G}}$ via the recovery map. We extend P_G to $\bar{\mathcal{G}}$ by assigning zero mass to \perp when comparing distributions across the two spaces.

Proposition 1 (Recovery is non-expansive in total variation (TV) distance). *For any sequence distributions Q_X, P_X on \mathcal{X} , the following inequality for the total variation distance d_{TV} holds:*

$$d_{\text{TV}}(\psi_{\#}Q_X, \psi_{\#}P_X) \leq d_{\text{TV}}(Q_X, P_X).$$

Proposition 2 (Bounded graph statistics inherit closeness). *For any bounded function $f : \bar{\mathcal{G}} \rightarrow \mathbb{R}$,*

$$|\mathbb{E}_{Q_G}f - \mathbb{E}_{P_G}f| \leq 2\|f\|_{\infty} d_{\text{TV}}(Q_G, P_G) \leq 2\|f\|_{\infty} d_{\text{TV}}(Q_X, P_X).$$

Choosing f as the indicator (or bounded support) of a fixed subgraph H , extended by $f(\perp) = 0$, shows that closeness in the sequence distribution implies closeness in subgraph statistics. Both propositions follow from the data-processing inequality and the dual characterization of total variation; short proofs are in Appendix B.

Corollary 3 (Non-identifiability of bounded subgraph statistics). *Let \hat{P}_G^{boot} denote the empirical (graph-level bootstrap) distribution on the training corpus $\{G_1, \dots, G_n\} \subseteq \mathcal{G}$. For any bounded function $f : \bar{\mathcal{G}} \rightarrow \mathbb{R}$ and any $\varepsilon > 0$, there exist sequence-level model distributions $Q_X^{(\text{mem})}$ and $Q_X^{(\text{gen})}$ such that $|\mathbb{E}_{Q_G^{(\text{mem})}}f - \mathbb{E}_{Q_G^{(\text{gen})}}f| < \varepsilon$, where $Q_G^{(\text{mem})}$ concentrates on $\{G_1, \dots, G_n\}$ (verbatim recall) and $Q_G^{(\text{gen})}$ places positive mass outside the training corpus.*

Corollary 3 is the operational reading of Propositions 1 and 2: agreement on any single bounded subgraph statistic, including support-based ranking and divergence summaries, cannot separate verbatim recall from distribution-level reproduction without a memorization reference. A generator should be considered to go *beyond* memorization only when its statistic lies outside the bootstrap reference distribution sampled from \hat{P}_G^{boot} . This pins down the central methodological point of the paper: *aggregate distributional metrics must be calibrated against memorization to be interpretable*, and motivates the two empirical axes, memorization rate and distributional alignment, that together place every generator on the *memorization–alignment spectrum* we adopt throughout the paper.

Bootstrap baseline as graph-level resampling. Given n training graphs G_1, \dots, G_n , the graph-level bootstrap estimator is $\hat{P}_G^{\text{boot}}(G) = \frac{1}{n} \sum_{i=1}^n \mathbf{1}[G = G_i]$, the empirical distribution. It places

mass only on training graphs: $\hat{P}_G^{\text{boot}}(G) = 0$ for any $G \notin \{G_1, \dots, G_n\}$. By contrast, an autoregressive model factorizes $Q_G(G) = Q_X(\phi(G)) = \prod_t Q(x_t | x_{<t})$, which can place positive mass on unseen graphs. The gap between *memorization-dominated* regimes ($Q_G \approx \hat{P}_G^{\text{boot}}$) and *distributional-generalization* regimes (Q_G deviates from \hat{P}_G^{boot} in a structurally meaningful direction) is what our calibrated protocol aims to expose.

4 Calibrated Evaluation Framework

We operationalize Corollary 3 as a concrete evaluation framework in this section. We first specify the graph serializations and training setup (§4.1), then define the subgraph statistics and whole-graph exact-match rate that serve as the basic observables of our diagnostic (§4.2). On top of these quantities, we introduce two primary diagnostics: a graph-level bootstrap calibration that provides an empirical memorization reference (§4.3), and a frequency-stratified analysis that identifies where alignment breaks down across the support distribution (§4.4). Together with the sequence-space hit/miss analysis reported in Appendix E, these diagnostics place each model on the memorization–alignment plane introduced in §3, rather than collapsing its behavior to a single aggregate fidelity score.

4.1 Graph Serialization and Training

We consider two well-established methods for serialization $\phi : \mathcal{G} \rightarrow \mathcal{X}$. **Canonical DFS code**, developed to efficiently enumerate subgraphs in gSpan [Yan and Han, 2002], runs a depth-first traversal of $G = (V, E, \ell_V, \ell_E)$ to emit edge tuples $t = \langle i, j, \ell_i, \ell_j, \ell_{ij} \rangle$ ($i < j$ forward, $i > j$ backward), totally orders tuple sequences lexicographically, and selects the minimum—the canonical DFS code $C_{\min}(G)$, unique up to graph isomorphism—which we serialize tuple-by-tuple with one token per tuple (rightmost-path construction in Algorithm 1, Appendix C). **DGMG action sequences** [Li et al., 2018] encode G as a sequential decision process (ADD_NODE, ADD_EDGE, DEST, END_EDGE, END_NODE); we canonicalize by adding nodes in sorted-label order so isomorphic graphs share the same action string. We train decoder-only LLaMA causal language models [Touvron et al., 2023] from scratch on the serialized sequences with the standard language modeling objective, minimizing the per-token negative log-likelihood (NLL). TU-benchmark training uses a fixed 80M-token budget; the PCQM4Mv2 schedule is in §5.

4.2 Subgraph Statistics via Frequent Pattern Mining

Let \mathbf{D}_{tr} and \mathbf{D}_{gen} denote the training and generated graph databases (finite samples from P_G and Q_G , respectively, in the notation of §3). We write $g \sqsubseteq G$ when g is a (vertex- and edge-labeled) subgraph of G , and define the *support* of a pattern g in a database \mathbf{D} as

$$\text{supp}_{\mathbf{D}}(g) = \frac{1}{|\mathbf{D}|} \sum_{G \in \mathbf{D}} \mathbf{1}[g \sqsubseteq G].$$

gSpan [Yan and Han, 2002] with minimum-support ratio $\sigma = 0.1$ enumerates all subgraphs whose supports are larger than σ , yielding the frequent-pattern sets \mathcal{P}_{tr} and \mathcal{P}_{gen} . We use their union $\mathcal{U} = \mathcal{P}_{\text{tr}} \cup \mathcal{P}_{\text{gen}}$ and intersection $\mathcal{C} = \mathcal{P}_{\text{tr}} \cap \mathcal{P}_{\text{gen}}$, and define support and normalized pattern probability for each $g \in \mathcal{U}$ as

$$s_{\text{tr}}(g) = \text{supp}_{\mathbf{D}_{\text{tr}}}(g), \quad p_{\text{tr}}(g) = \frac{s_{\text{tr}}(g)}{\sum_{h \in \mathcal{U}} s_{\text{tr}}(h)},$$

and analogously $s_{\text{gen}}, p_{\text{gen}}$ on \mathbf{D}_{gen} .

Distributional metrics. We quantify the alignment of \mathcal{P}_{gen} to \mathcal{P}_{tr} using four scalar summaries: *Spearman’s ρ* is the rank correlation between s_{tr} and s_{gen} restricted to the intersection \mathcal{C} , capturing preservation of the relative frequency ordering. *Jensen–Shannon divergence* (JSD) is $\text{JSD}(p_{\text{tr}}, p_{\text{gen}}) = \text{KL}(p_{\text{tr}} \| m) / 2 + \text{KL}(p_{\text{gen}} \| m) / 2$ with mid-point $m = (p_{\text{tr}} + p_{\text{gen}}) / 2$. The training-side *missing mass* $\text{MM} = \sum_{g \in \mathcal{P}_{\text{tr}} \setminus \mathcal{P}_{\text{gen}}} p_{\text{tr}}(g)$ records the probability mass on patterns absent from the generated set; the generated-side *novel mass* $\text{NM} = \sum_{g \in \mathcal{P}_{\text{gen}} \setminus \mathcal{P}_{\text{tr}}} p_{\text{gen}}(g)$ is its complement on patterns absent from training.

Whole-graph memorization. At the whole-graph level we measure verbatim recall through canonical-DFS-code equality: writing $\text{code}(\mathbf{D}) = \{\text{code}(G) : G \in \mathbf{D}\}$,

$$\text{EM} = \frac{|\{G \in \mathbf{D}_{\text{gen}} : \text{code}(G) \in \text{code}(\mathbf{D}_{\text{tr}})\}|}{|\mathbf{D}_{\text{gen}}|}, \quad \text{Novelty} = 1 - \text{EM}. \quad (1)$$

The exact-match rate EM, reported as “precision” in result tables for backwards compatibility, is the empirical counterpart of the bootstrap estimator \hat{P}_G^{boot} of §3: when the model collapses onto memorized training graphs, $Q_G \approx \hat{P}_G^{\text{boot}}$ and $\text{EM} \rightarrow 1$.

From Propositions to Protocol. We introduce the two diagnostics in the following subsections, which are not independent benchmarks but operational projections of Corollary 3. The graph-level bootstrap (§4.3) realizes the memorization reference \hat{P}_G^{boot} empirically, so that comparing a model’s ρ or JSD against the bootstrap distribution tests the exact ambiguity the Corollary forbids one to ignore. Frequency stratification (§4.4) sharpens Proposition 2 by restricting the test function f to a support sub-band, exposing where aggregate ρ hides a structural deficit. As a complementary sequence-space check, per-sequence NLL hit/miss (Appendix E) is the sequence-space counterpart of Proposition 1: it asks whether the TV gap concentrates on the precise sequences the model later reproduces. Reading the three diagnostics jointly returns a verdict on the two-dimensional memorization–alignment plane rather than another scalar fidelity number.

4.3 Bootstrap Calibration

A high Spearman ρ between training and generated sets may simply reflect the fact that most generated graphs are drawn from the training distribution via memorization. To calibrate this, we construct a bootstrap baseline that samples directly from the graph-level estimator \hat{P}_G^{boot} of §3 as an empirical memorization reference: it estimates the distributional alignment expected when generated graphs are drawn directly from the training corpus. Concretely, for $R = 10$ repeats we draw $|\mathbf{D}_{\text{gen}}|$ training graphs with replacement, run gSpan on each resample, and compute $\rho^{(r)}$, $\text{JSD}^{(r)}$, $\text{MM}^{(r)}$ against \mathcal{P}_{tr} (full pseudo code in Algorithm 2, Appendix C). We report the model’s percentile rank within the resulting bootstrap distribution and the calibrated z -score $z = (\rho_{\text{model}} - \mu_{\text{boot}}) / \sigma_{\text{boot}}$.

4.4 Frequency-Stratified Analysis

Aggregate metrics over \mathcal{U} obscure how alignment varies with pattern frequency, which is exactly the regime where memorization-driven and structurally-learned models diverge most. We therefore sort the training patterns \mathcal{P}_{tr} by support s_{tr} and partition them into a *Head* (top 10%, high-frequency motifs that dominate the distribution), a *Torso* (middle 80%, moderately frequent patterns), and a *Tail* (bottom 10%, rare patterns near the support threshold). Within each stratum we recompute Spearman ρ , JSD, and MM on the corresponding restriction of \mathcal{U} , so that any frequency-dependent generalization gap—typically a Head/Torso–Tail split—becomes directly visible rather than averaged out.

As a complementary per-sequence check, we compute average per-token NLL under the model for every unique training sequence and compare *hits* (reproduced in generation) against *misses* (not reproduced) via the Mann–Whitney U test (full results in Appendix E).

5 Experimental Setup

We evaluate on five TU benchmarks [Morris et al., 2020] and the PCQM4Mv2 molecular corpus from OGB-LSC [Hu et al., 2021] (per-dataset graph statistics in Appendix H, Table 9); PCQM4Mv2 contributes 3,746,620 graphs with a canonical-DFS training split of 3,371,958 sequences (3,104,677 unique after deduplication). Models are LLaMA [Touvron et al., 2023] SMALL (132M parameters; 12 layers, hidden 768, 12 heads, FFN 3072) trained from scratch with causal LM, TRL SFTTrainer + DeepSpeed ZeRO-1 [Rajbhandari et al., 2020], AdamW [Loshchilov and Hutter, 2019] ($\text{lr} = 10^{-5}$), cosine schedule, bf16, an 80M-token budget, and 20 evenly spaced checkpoints; for each TU dataset we train one DFS-canonical and one DGMG model. PCQM4Mv2 additionally sweeps TINY/MEDIUM/LARGE variants (10.5M–451M parameters; PCQM4Mv2 scaling results below). For each model we sample 1024 sequences under six decoding configurations (default `both_default`):

Table 1: Generation metrics under `both_default` decoding (DFS canonical, single training seed = 42; ENZYMES values are means over 5 decoding seeds under the no-cap gBolt rerun, see Limitations (g)). Whole-graph: Unique, Precision (= EM, Eq. (1)), Novelty. Subgraph-level: $|\mathcal{P}_{\text{tr}}|$ and $|\mathcal{P}_{\text{gen}}|$ are gSpan subgraph pattern set sizes, ρ Spearman rank correlation, JSD Jensen–Shannon divergence, Missing the training-side missing mass.

| Dataset | Unique | Precision | Novelty | $ \mathcal{P}_{\text{tr}} $ | $ \mathcal{P}_{\text{gen}} $ | ρ | JSD | Missing |
|----------|--------|-----------|---------|-----------------------------|------------------------------|--------|-------|---------|
| MUTAG | 0.199 | 0.828 | 0.172 | 634 | 714 | 0.976 | 0.035 | 0.014 |
| PTC_MR | 0.285 | 0.983 | 0.017 | 127 | 148 | 0.950 | 0.063 | 0.007 |
| ENZYMES | 0.418 | 1.000 | 0.000 | 95,419 | 101,710 | 0.987 | 0.014 | 0.007 |
| PROTEINS | 0.591 | 0.891 | 0.109 | 70,257 | 75,859 | 0.988 | 0.022 | 0.005 |
| NCII | 0.862 | 1.000 | 0.000 | 818 | 884 | 0.990 | 0.010 | 0.006 |

$T = 1.0$, $\text{top-}p = 0.95$, $\text{top-}k = 50$; full sweep in Appendix L), parse them into graphs (regex for DFS, action parsing for DGMG), and run the evaluation pipeline of §4: gSpan ($\sigma = 0.1$), distributional metrics, bootstrap baselines, subgraph pattern strata, NLL hit/miss, and Weisfeiler–Lehman (WL) kernel MMD [Shervashidze et al., 2011]. Serialized-sequence length and vocabulary statistics are in Appendix H (Table 10).

6 Results

Diagnostic expectations. The framework of §4 commits to four concrete expectations; the TU/PCQM regimes below are read against them rather than reverse-engineered from the tables.

(E1) Under Corollary 3, a memorization-dominated regime places ρ inside the graph-level bootstrap reference, making subgraph-level aggregate fidelity uninformative (calibrated baseline comparison below).

(E2) A regime that goes beyond memorization retains ρ when gSpan is restricted to the novel-only subset $\mathbf{D}_{\text{gen}} \setminus \mathbf{D}_{\text{tr}}$, so the subgraph-level alignment is not carried by whole-graph recall alone (PCQM4Mv2 scaling below).

(E3) Frequency stratification exposes, rather than averages over, support deficits hidden by aggregate ρ (frequency-stratified analysis below).

(E4) If the capacity is structural, the same crossover is reproduced under a distinct serialization rather than tied to a specific tokenization (PCQM4Mv2 scaling below; Appendix I.2).

Overall distribution alignment. Table 1 presents the primary generation metrics under `both_default` decoding for all datasets in canonical DFS code format.

Across all datasets, Spearman correlations are remarkably high ($\rho = 0.950\text{--}0.990$), indicating that the relative ordering of frequent subgraph patterns is well-preserved in the generated sets. Missing mass is uniformly low ($< 1.5\%$), suggesting that most training patterns are reproduced. However, two observations complicate this optimistic subgraph-level reading. First, at the *whole-graph* level, verbatim memorization rates are high: 82.8%–100% of generated sequences are exact matches of training graphs (precision in Table 1, EM of Eq. (1)). NCII achieves $\rho = 0.990$ with 100% precision (zero novelty), meaning every generated graph was already present in training corpus. Second, generated-set *whole-graph* uniqueness rates inversely correlate with *whole-graph* memorization: MUTAG generates only 19.9% unique sequences (heavy duplication), while NCII achieves 86.2%, reflecting its larger training set.

Standard label-free MMD metrics give the same optimistic reading ($< 3 \times 10^{-3}$ for every TU benchmark; full breakdown in Appendix G, including a cross-model comparison that shows label-free MMD hiding the labeled-structure failure of unlabeled baselines that WL exposes), but Cor 3 shows that such aggregate agreement is compatible with both memorization and structural learning, motivating the bootstrap calibration below. Distributional metrics are also strongly modulated by decoding configuration—inter-config ρ spread can exceed 0.3, large enough to shift the bootstrap-calibrated verdict (full sweep in Appendices L, F); the main text reports `both_default`.

Table 2: Model vs. bootstrap baseline (single training seed = 42; ENZYMES values are aggregated over 5 decoding seeds \times 10 bootstrap repeats under the no-cap gBolt rerun to match the no-cap audit in Limitations (g)). $\Delta\rho$: model Spearman minus bootstrap median. z : standardized score. Pctile: percentile rank of model within bootstrap distribution. Values below the bootstrap median are highlighted in red.

| Dataset | ρ | $\Delta\rho$ | $z(\rho)$ | Pctile | JSD | Boot JSD |
|----------|--------|--------------|-----------|--------|-------|----------|
| MUTAG | 0.976 | -0.014 | -2.54 | 0% | 0.035 | 0.021 |
| PTC_MR | 0.950 | -0.023 | -1.49 | 10% | 0.063 | 0.022 |
| ENZYMES | 0.987 | -0.005 | -2.78 | 4% | 0.014 | 0.010 |
| PROTEINS | 0.988 | +0.005 | +0.62 | 60% | 0.022 | 0.016 |
| NCII | 0.990 | +0.000 | +0.43 | 50% | 0.010 | 0.012 |

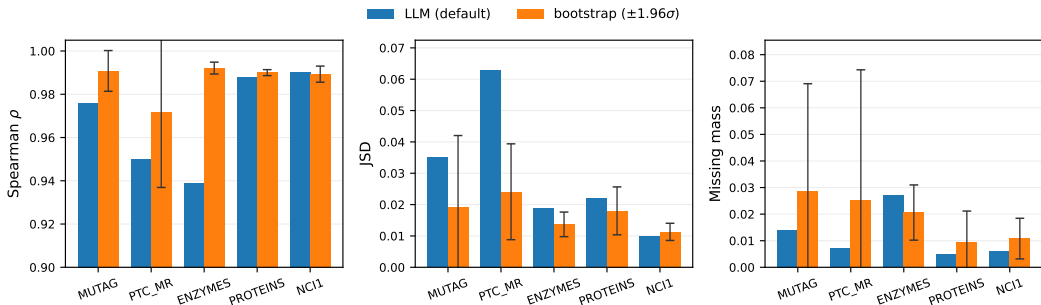


Figure 1: LLM (DFS canonical, both_default, single training seed = 42) vs. graph-level bootstrap baseline on the five TU benchmarks. Bars on each panel show the model and bootstrap mean; error bars on the bootstrap bar are $\pm 1.96\sigma$ over 10 bootstrap repeats (a Gaussian approximation of a 95% band; the raw 5–95 percentile would be too noisy at $n_{\text{boot}} = 10$). Bootstrap matches or exceeds the model on Spearman ρ for MUTAG, PTC_MR, and ENZYMES, and is competitive with the model on JSD and missing mass throughout, visualizing the calibrated reading of Table 2.

Calibrated baseline comparison. Table 2 compares model metrics against bootstrap baselines, which represent the distributional alignment achievable by simply resampling from the training set.

Key finding: High ρ is within the bootstrap range. For MUTAG, PTC_MR, and ENZYMES, the model’s Spearman ρ falls *below* the bootstrap median ($\Delta\rho < 0$), placing the model below the bootstrap distribution’s center on these three datasets (negative $z(\rho)$ throughout, with ENZYMES the most negative under the tight no-cap bootstrap reference even though its $|\Delta\rho|$ is smallest). For PROTEINS and NCII, the model is at or slightly above the bootstrap median, but within the bootstrap band shown in Figure 1. This result implies that the high distributional alignment observed in Table 1 is largely a statistical consequence of memorization: if the model reproduces most training graphs, the subgraph distribution alignment follows trivially. *High ρ alone cannot be interpreted as evidence of structural learning beyond memorization.*

The DGMG serialization shows a similar pattern (Appendix D, Table 4), with PROTEINS-DGMG and (under no-cap gBolt; Limitations (g)) ENZYMES-DGMG nominally exceeding the bootstrap at the 100th and 80th percentile ($z = +1.49$ and $+0.69$).¹

Frequency-stratified analysis. The aggregate metrics mask a dramatic frequency-dependent structure. Figure 2 presents the per-stratum breakdown; full numeric values are reported in Appendix I.1 (Table 13).

Head and Torso strata are reproduced with high fidelity (missing mass $\leq 0.8\%$ and $\rho \geq 0.91$ in every condition), but the Tail stratum shows substantial coverage failures: missing mass climbs to 13.5–22.0%, an order of magnitude larger than the Head/Torso gap. Rank correlation on the patterns the model does produce (intersection-Spearman Tail $\rho \in [0.26, 0.56]$, mean over $n = 5$ decoding-seed reruns) sits well below the $\rho \geq 0.97$ achieved on Head/Torso. Tail estimates are themselves

¹The absolute gaps are small ($\Delta\rho = +0.009$ and $+0.001$), within decoding-seed variability, so neither is strong evidence of structural learning beyond memorization; see Appendix D.

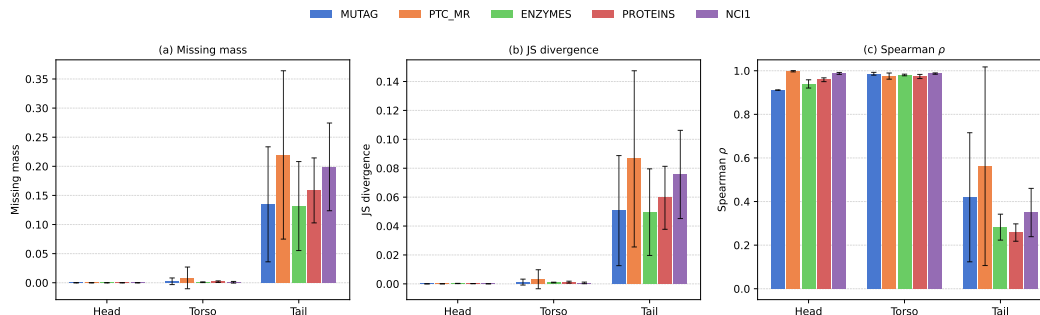


Figure 2: Frequency-stratified metrics (DFS canonical, single training seed = 42), bar heights = mean over $n = 5$ decoding-seed reruns of the same LLaMA-SMALL (132M) checkpoint, error bars = sample standard deviation. Missing mass and Spearman ρ are *independent* diagnostics: missing mass measures *coverage* (what fraction of stratum mass is omitted), while ρ measures *rank* on the patterns the model does emit. Head/Torso are reproduced with high fidelity and tight error bars across all decoding seeds; Tail patterns exhibit elevated missing mass and Jensen–Shannon divergence, and lower Spearman rank correlation, with substantially wider error bars—reflecting that 1024 samples are too few to densely cover the bottom-decile pattern set (per-seed numbers in Appendix I.4).

noisy across decoding seeds—PTC_MR and MUTAG Tail ρ swing by ± 0.30 – 0.46 across reruns—reflecting that 1024 samples are too few to densely cover the bottom-decile pattern set; per-seed values, the more stable *trainkeys* variant (filling omitted patterns with zero), and the per-dataset Head–Tail gap $\Delta\rho$ are reported in Appendices I.4–I.3. This is a *frequency-dependent generalization gap*: the model concentrates mass on frequent motifs and systematically under represents rare ones, with sampling alone unable to recover the distribution’s tail at the available decoding budget.

Two diagnostic checks corroborate the whole-graph memorization reading of the calibrated baseline comparison above: an NLL hit/miss test (Mann–Whitney U , $p < 10^{-5}$ on ENZYMES/NCI1; Appendix E) and a one-way variance decomposition where decoding explains 57–71% of Spearman variance and training progress dominates missing-mass variance ($> 76\%$; Appendix F). Repeating the protocol with DGMG action sequences yields serialization-consistent aggregate patterns (WL-MMD < 0.006 , coverage > 0.92 , DGMG memorization \geq DFS in every dataset; Appendix H) and reproduces the qualitative Head–Tail gap (Appendix I.2), while per-dataset bootstrap percentiles vary between serializations (Appendix D)—qualitative evidence for expectation (E4), robustness across the two serializations.

Structural baselines. Against three structural baselines, **DiGress** [Vignac et al., 2023] (discrete denoising diffusion), **GraphRNN** [You et al., 2018b], and **DGMG-official** [Li et al., 2018], DiGress occupies a low whole-graph memorization but lower subgraph-level alignment regime (recall $\leq 2\%$, $\rho \in [0.62, 0.93]$), confirming that high ρ does not require memorization. GraphRNN and DGMG-official, being label-unaware, fail to recover labeled gSpan support on most TU datasets and leave ρ undefined, even though their unlabeled degree/orbit MMD match training (full per-model numbers in Appendix N, Table 21; cross-model MMD aggregate in Appendix G). High ρ alone is therefore insufficient as a verdict, and the LLM’s near-perfect TU alignment still requires the bootstrap calibration above.

Scaling to PCQM4Mv2. Propositions 1–2 establish that high ρ is consistent with memorization; the empirical question is whether the converse—high ρ *without* near-complete verbatim recall of the corpus—arises at scale, where memorizing 3.10M unique training sequences becomes substantially harder at fixed ~ 132 M-parameter capacity. Applying the same DFS pipeline to PCQM4Mv2, exact-match recall *at the whole-graph level* drops to 31.7% while *subgraph-level* Spearman remains high ($\rho = 0.976$, JSD = 0.044, uniqueness = 1.000); the full scale-comparison is in Appendix P (Table 29). The TU bootstrap is uninformative at this scale; a novel-only subset analysis on a fixed 10,000-graph subsample tracks the all-generation Spearman within 0.026 across the capacity sweep (Appendix P). The Tail stratum still degrades sharply (Tail $\rho = 0.41 \pm 0.22$, missing mass 0.07 ± 0.02 ; Table 3), while same-corpus DiGress collapses uniformly (Head missing mass already 0.47, Head $\rho = 0.54$), so the “rare-pattern-only” failure mode is specific to the LLM regime. Aggregate whole-

Table 3: PCQM4Mv2 Tail-stratum diagnostics (single training seed = 42; mean \pm std over 5 random 10k training-reference subsamples; reference-side variance only). LLM-DFS preserves Head/Torso almost perfectly and loses ground only in the Tail; DiGress collapses uniformly. Full breakdown and decoding-stage variance discussion in Appendix P (Table 31).

| Model | Tail Missing | Tail JSD | Tail ρ |
|---------|-------------------|-------------------|-------------------|
| LLM-DFS | 0.069 ± 0.017 | 0.026 ± 0.006 | 0.406 ± 0.222 |
| DiGress | 0.860 ± 0.033 | 0.489 ± 0.029 | 0.046 ± 0.212 |

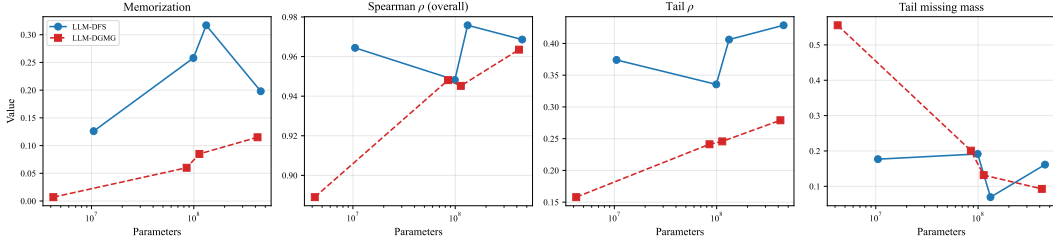


Figure 3: Cross-model PCQM4Mv2 scaling. Memorization, overall ρ , Tail ρ , and Tail missing mass plotted against parameter count for LLM-DFS (4 sizes, blue) and LLM-DGMG (4 sizes, red). Distribution-alignment metrics sit in a narrow band across the $43\times$ DFS sweep, while memorization and missing mass move with capacity. The DGMG four-point sweep reproduces the same trend under a different serialization.

graph MMDs stay in the same low band as on TU (Appendix G)—a regime where Cor 3 makes the bootstrap and stratification of §4 the load-bearing diagnostics, not aggregate MMD.

Capacity sweep and cross-serialization robustness. The DFS capacity sweep (10.5M–451M, $43\times$) on PCQM4Mv2 leaves subgraph-level $\rho \in [0.95, 0.98]$ and whole-graph WL-MMD $\in [0.0014, 0.0023]$ in narrow bands, with Tail ρ peaking at ≈ 0.43 . A four-point DGMG sweep exhibits the same capacity-dependent trends under a different serialization (Figure 3, Appendix P), supporting expectation (E4)—robustness across the two serializations we test.

7 Discussion and Conclusion

Our results suggest a conditional answer to our central question—whether graph language models go beyond memorization: yes, but only at sufficient scale and primarily for frequent substructures.

On small TU benchmarks, high subgraph-level alignment is largely explained by whole-graph memorization: the model’s Spearman correlation falls within, or close to, the distribution induced by a non-learning bootstrap baseline. In this regime, aggregate fidelity is therefore not evidence of structural acquisition. At PCQM4Mv2 scale, however, the regime shifts. Exact-match recall drops sharply, yet the generated graphs preserve the rank structure of frequent subgraph statistics, even when evaluation is restricted to novel-only generations. This decoupling between whole-graph recall and subgraph-level alignment provides evidence that autoregressive graph language models can internalize structural regularities rather than merely replay training graphs. The same qualitative crossover appears under both canonical DFS codes and DGMG action sequences, suggesting it is not a serialization artifact. By contrast, non-LLM baselines occupy different territory: the label-aware DiGress baseline achieves no exact-match recall yet also fails to recover frequent-subgraph distributions, while label-unaware baselines (GraphRNN, DGMG-official) cannot share the labeled support that defines alignment (§6, structural baselines). High subgraph-level alignment with low whole-graph recall therefore appears specific to large-scale graph language models in our scope.

This structural acquisition is uneven: Head and Torso patterns are reproduced reliably while Tail patterns remain poorly covered across datasets and serializations, so *graph language models behave as implicit neural graph miners only in a partial sense—recovering the dominant support structure but not the rare-substructure tail*. Memorization-aware diagnosis thus requires a non-learning reference and frequency-stratified evaluation; Tail coverage is the natural next step.

Acknowledgments

This work was supported by JSPS, KAKENHI Grant Number JP25H01112, Japan and JST, CREST Grant Number JPMJCR22D3, Japan.

References

- Viraj Bagal, Rishal Aggarwal, P K Vinod, and U Deva Priyakumar. MolGPT: Molecular generation using a transformer-decoder model. *Journal of Chemical Information and Modeling*, 62(9):2064–2076, 2022.
- Nicholas Carlini, Florian Tramer, Eric Wallace, Matthew Jagielski, Ariel Herbert-Voss, Katherine Lee, Adam Roberts, Tom Brown, Dawn Song, Ulfar Erlingsson, et al. Extracting training data from large language models. In *30th USENIX Security Symposium*, 2021.
- Nicholas Carlini, Daphne Ippolito, Matthew Jagielski, Katherine Lee, Florian Tramer, and Chiyuan Zhang. Quantifying memorization across neural language models. In *International Conference on Learning Representations*, 2023.
- Dexiong Chen, Markus Krimmel, and Karsten Borgwardt. Flatten graphs as sequences: Transformers are scalable graph generators. *arXiv preprint arXiv:2502.02216*, 2025. URL <https://arxiv.org/abs/2502.02216>.
- Bahare Fatemi, Jonathan Halcrow, and Bryan Perozzi. Talk like a graph: Encoding graphs for large language models. In *International Conference on Learning Representations*, 2024.
- Nikhil Goyal, Harsh Vardhan Jain, and Sayan Ranu. Graphgen: A scalable approach to domain-agnostic labeled graph generation. In *Proceedings of The Web Conference 2020*, pages 1253–1263, 2020.
- Weihua Hu, Matthias Fey, Hongyu Ren, Maho Nakata, Yuxiao Dong, and Jure Leskovec. OGB-LSC: A large-scale challenge for machine learning on graphs. In *NeurIPS Datasets and Benchmarks Track*, 2021.
- Jaehyeong Jo, Seul Lee, and Sung Ju Hwang. Score-based generative modeling of graphs via the system of stochastic differential equations. In *International Conference on Machine Learning*, 2022.
- Yujia Li, Oriol Vinyals, Chris Dyer, Razvan Pascanu, and Peter W. Battaglia. Learning deep generative models of graphs. *arXiv preprint arXiv:1803.03324*, 2018.
- Ilya Loshchilov and Frank Hutter. Decoupled weight decay regularization. In *International Conference on Learning Representations*, 2019.
- Christopher Morris, Nils M. Kriege, Franka Bause, Kristian Kersting, Petra Mutzel, and Marion Neumann. TUDataset: A collection of benchmark datasets for learning with graphs. In *ICML 2020 Workshop on Graph Representation Learning and Beyond (GRL+)*, 2020.
- Chenhao Niu, Yang Song, Jiaming Song, Shengjia Zhao, Aditya Grover, and Stefano Ermon. Permutation invariant graph generation via score-based generative modeling. In *Proceedings of the 23rd International Conference on Artificial Intelligence and Statistics*, 2020.
- Samyam Rajbhandari et al. ZeRO: Memory optimizations toward training trillion parameter models. In *Proceedings of the International Conference for High Performance Computing, Networking, Storage and Analysis*, 2020.
- Clayton Sanford, Bahare Fatemi, Ethan Hall, Anton Tsitsulin, Mehran Kazemi, Jonathan Halcrow, Bryan Perozzi, and Vahab Mirrokni. Understanding transformer reasoning capabilities via graph algorithms. In *Advances in Neural Information Processing Systems*, 2024.
- Nino Shervashidze, Pascal Schweitzer, Erik Jan van Leeuwen, Kurt Mehlhorn, and Karsten M. Borgwardt. Weisfeiler-lehman graph kernels. *Journal of Machine Learning Research*, 12(77):2539–2561, 2011. URL <http://jmlr.org/papers/v12/shervashidze11a.html>.

- Chence Shi, Minkai Xu, Zhaocheng Zhu, Weinan Zhang, Ming Zhang, and Jian Tang. GraphAF: a flow-based autoregressive model for molecular graph generation. In *International Conference on Learning Representations*, 2020.
- Martin Simonovsky and Nikos Komodakis. GraphVAE: Towards generation of small graphs using variational autoencoders. In *International Conference on Artificial Neural Networks*, 2018.
- Gowthami Somepalli, Vasu Singla, Micah Goldblum, Jonas Geiping, and Tom Goldstein. Diffusion art or digital forgery? investigating data replication in diffusion models. In *IEEE/CVF Conference on Computer Vision and Pattern Recognition*, 2023.
- Rylee Thompson, Boris Knyazev, Elahe Ghalebi, Jungtaek Kim, and Graham W. Taylor. On evaluation metrics for graph generative models. In *International Conference on Learning Representations*, 2022.
- Hugo Touvron et al. LLaMA: Open and efficient foundation language models. *arXiv preprint arXiv:2302.13971*, 2023.
- Clement Vignac, Igor Krawczuk, Antoine Siraudin, Bohan Wang, Volkan Cevher, and Pascal Frossard. Digress: Discrete denoising diffusion for graph generation. In *International Conference on Learning Representations*, 2023.
- Xifeng Yan and Jiawei Han. gspan: Graph-based substructure pattern mining. In *Proceedings of the IEEE International Conference on Data Mining (ICDM)*, pages 721–724. IEEE, 2002. doi: 10.1109/ICDM.2002.1184038.
- Jiaxuan You, Bowen Liu, Rex Ying, Vijay Pande, and Jure Leskovec. Graph convolutional policy network for goal-directed molecular graph generation. In *Advances in Neural Information Processing Systems*, 2018a.
- Jiaxuan You et al. Graphrnn: Generating realistic graphs with deep auto-regressive models. In *Proceedings of the 35th International Conference on Machine Learning*, 2018b.
- Qifang Zhao, Weidong Ren, Tianyu Li, Hong Liu, Xingsheng He, and Xiaoxiao Xu. Graphgpt: Generative pre-trained graph eulerian transformer. *arXiv preprint arXiv:2401.00529*, 2024. URL <https://arxiv.org/abs/2401.00529>.
- Keren Zhou. gBolt: a C++ implementation of the gspan algorithm. <https://github.com/Jokeren/gBolt>, 2017. BSD 2-Clause License.

Reproducibility Statement

We aim to make every reported number reproducible from the public companion repository.

Datasets. TU-benchmark graphs (MUTAG, ENZYMES, NCI1, PROTEINS, PTC_MR) are obtained through PyTorch Geometric’s TUDataset loader using the canonical splits. PCQM4Mv2 is obtained from the OGB v1.3.5 release; we use the 2D-graph-only split. All preprocessing (DFS-code conversion, DGMG action sequence construction, and gSpan pattern extraction with $\sigma = 0.1$, executed via a patched gBolt [Zhou, 2017] C++ engine—max-vertices cap, projection-memory safeguard, and extended DFS-code output for canonical-form parity with the reference Python gSpan—wrapped by an anonymized Python interface) is included in the companion repository.

Hardware. All reported experiments run on a single NVIDIA A100 80 GB (PCIe) with bf16 mixed precision via DeepSpeed ZeRO-1. Per TU dataset, training to 80M non-padding tokens takes ≈ 5.5 GPU-hours at ≈ 11 it/s with batch size 16 (DGMG: 4). The multi-seed TU sweep (5 datasets \times 2 serializations \times 2 seeds = 20 runs, including the seed=42 run) amounts to ≈ 110 GPU-hours; PCQM4Mv2 (single seed) adds the same order of magnitude depending on epoch count and model size. Beyond these headline figures, preliminary architecture and hyperparameter sweeps over LLaMA sizes, decoding-configuration ablations, and DeepSpeed/serialization debugging—together with abandoned and failed runs that were not retained for the final analysis—approximately doubled the total project compute. We do not report exact wall-clock for these exploratory runs because logs of failed and discarded configurations were not systematically preserved; the companion repository contains only the configurations and seeds used for the reported numbers.

Seeds. Training uses a global seed (42, 1337, 2024 for the three TU runs), passed through to `transformers.set_seed` and to the SFT trainer (`seed` and `data_seed`). PCQM4Mv2 uses a single seed (42) due to compute budget; its variance is documented qualitatively in the limitations. Generation samplers expose their own seed through the evaluation pipeline.

Confidence intervals. The main-text TU tables report mean \pm sample std over $n = 5$ decoding seeds at training seed = 42; the same checkpoint is fixed across decoding draws so the variance reflects sampling noise alone (per-dataset breakdown in Appendix I.4, Table 16). A full two-way ablation across both training seeds {42, 1337} and the same five decoding seeds (100 evaluations) is reported in Table 24 and shows that the training-seed shift on the decoding-mean is bounded by 0.05 on Tail miss and 0.10 on Tail ρ_{\cap} , inside the decoding-seed std on every cell—i.e. decoding-stage noise dominates training-seed noise. The seed-2024 run is queued and will close the $n=3$ Student- t aggregate at the camera-ready stage. Bootstrap baselines on TU use 10 resamples and report $\pm 1.96\sigma$ bands; PCQM4Mv2 is single-training-seed by design, its larger reference set ($\sim 10^4$ tail patterns) absorbs most sampling noise, and we quote 5-subsample standard errors where applicable. Tables and figures are produced automatically from the aggregated artifacts.

Code release. Code and training scripts will be released under the MIT License at the (currently anonymized) URL listed in the supplementary material upon acceptance. The repository includes a single-command re-run script that idempotently trains, evaluates, and exports LaTeX tables and figures for the full benchmark matrix.

Broader Impact

Autoregressive generators of molecular and protein-interaction graphs share the dual-use profile of generative models in chemistry more broadly: a model that learns to extend small fragments into novel valid molecules could in principle be redirected toward toxic or controlled-substance design. Two factors mitigate the immediate risk in this work. First, our released models are trained on public academic graph benchmarks (TUDatasets and the OGB PCQM4Mv2 split) without property conditioning for toxicity, potency, or controlled-substance objectives. Second, the central scientific contribution is a calibrated evaluation framework for graph language models—a diagnostic for memorization vs structural alignment—rather than a stronger generator; the framework is equally useful for auditing generators with safety properties (e.g., flagging memorization of restricted training molecules) as for building them. We nonetheless recommend that downstream practitioners extending these methods to property-conditioned chemistry benchmarks adopt access controls and standard safety filters before releasing generators or generated samples.

A Limitations

(a) Serialization dependence. Memorization detection is string-based and therefore serialization-dependent. We test two formats (canonical DFS code and DGMG action sequences) and report the cross-serialization agreement as robustness evidence rather than a serialization-invariance claim (Appendix H); broader serialization sensitivity (SMILES, random walks, adjacency-based formats) and a graph-isomorphism-based detector are left for future work.

(b) Compute-optimal scaling. LARGE (451M for DFS, 419.7M for DGMG) is trained for 12 epochs under a fixed compute budget while TINY/MEDIUM/SMALL use 50 epochs (DFS) or 20 epochs (DGMG), so tokens-per-parameter is not held constant (9 tok/param for DFS-LARGE, 5.8 for DGMG-LARGE). The Tail-stratum gains at LARGE are therefore likely a lower bound under both serializations. A controlled compute-optimal scaling analysis over model size, data size, and training compute is left for future work.

(c) Multi-seed coverage. We separate two distinct sources of stochasticity: *training-seed* variance (different fine-tuning runs) and *decoding-seed* variance (different sampling draws from the same trained checkpoint), and characterize both via a full two-way ablation (Appendix O, Table 24): for every TU dataset and serialization, both training seeds {42, 1337} are evaluated under five fixed decoding seeds {0, 1, 2, 3, 4} (10 cells \times 5 = 50 draws per condition, 100 total). Decoding-stage noise dominates on TU: across all 10 cells the decoding-mean shift between training seeds is at most 0.05 on Tail miss and 0.10 on Tail ρ_{\cap} , inside the decoding-seed std band on every cell. This

empirically validates reporting decoding-seed averages throughout the paper and makes the seed-2024 camera-ready run a confirmation rather than a load-bearing addition. PCQM4Mv2 is single-training-seed; the larger reference set ($\sim 10^4$ tail patterns vs $\sim 10^2$ on TU) makes decoding-seed variance substantially smaller, but a full multi-seed PCQM4Mv2 sweep is deferred to the camera-ready stage.

(d) Structural baselines. Our reference baselines are graph-level bootstrap resamples, which preserve full graph structure. Degree-preserving randomization or configuration-model baselines would quantify how much structural information is needed to reach similar distributional alignment.

(e) gSpan sensitivity. We swept `min_sup` ($\sigma \in \{0.01, 0.1\}$) on three TU datasets (Appendix J) and found consistent conclusions, but `upper` (maximum subgraph size) is fixed and remains unexplored; a systematic sweep over both gSpan thresholds is left for future work, so Tail-stratum claims should be read as anchored to the (σ, upper) values used here.

(f) DGMG canonicalization is action-canonical, not isomorphism-canonical. The sorted-label canonicalization used for DGMG action sequences (§4.1) is deterministic but does not enumerate graph automorphisms; same-label nodes admitting non-trivial automorphisms can therefore yield distinct action strings even for isomorphic graphs. The DGMG memorization rates in Table 12 are computed on canonicalized action strings rather than isomorphism classes, so they lower-bound the true isomorphism-based recall. The DFS canonical code, in contrast, is unique up to graph isomorphism by construction [Yan and Han, 2002], so the DFS-side EM in Eq. (1) matches isomorphism-based recall.

(g) Projection-size memory guard in our patched gBolt. Our patched gBolt engine (§7) applies a fixed `MAX_PROJECTION_SIZE` of 5×10^5 occurrences: when an intermediate pattern’s projection exceeds this threshold, the corresponding search branch is skipped to prevent memory exhaustion on dense corpora. The guard primarily prunes extensions of small, high-multiplicity seed patterns; rare-substructure descendants (the Tail stratum, low-projection by construction) are largely unaffected by the guard, as we verify empirically below. Because the same pipeline is applied to training, generated, and bootstrap corpora, the relative metrics on the shared support—Spearman ρ , JSD, missing mass, and the bootstrap calibration—are unaffected in expectation, and our central claims (memorization regime on TU, decoupling on PCQM4Mv2, persistent Tail deficit, cross-serialization agreement) do not depend on the guard. The absolute pattern counts $|\mathcal{P}_{\text{tr}}|$ and $|\mathcal{P}_{\text{gen}}|$ reported in Table 1 should be read as implementation-side bounds: on ENZYMES the no-cap value of $|\mathcal{P}_{\text{tr}}|$ is $\approx 0.09\%$ larger (+84 patterns out of 95,335) and we report those values in Table 13; on PROTEINS the no-cap-to- 10^7 shift is $\approx 2.7\%$ and we keep the default-cap values because the ratio metric on the shared support cancels (see below); the four remaining datasets (MUTAG, PTC_MR, NCI1, PCQM4Mv2) are unaffected by the guard.

We further verified this empirically across all six paper datasets. Rerunning the full evaluation pipeline with the guard raised to 10^9 (effectively no cap) on MUTAG, PTC_MR, NCI1, ENZYMES, and the PCQM4Mv2 subsamples, and to 10^7 on PROTEINS (the no-cap binary exhausts memory on PROTEINS’ denser projections; the 10^7 value is $20\times$ the original 5×10^5 cap and suffices to expose the asymmetric vs symmetric distinction we report), we observe:

| Dataset | Patterns affected by guard | Head ρ shift |
|---------------------------------------|----------------------------|-------------------|
| MUTAG, PTC_MR, NCI1 | 0 | 0 |
| PCQM4Mv2 (10k subsample, 5 \times) | 0 | 0 |
| PROTEINS | 1,955 (2.7%) | -0.001 |
| ENZYMES | 90 (0.09%) | +0.152 |

The guard does not activate on three TU benchmarks or on PCQM4Mv2. PROTEINS shows a 2.7% pattern shift but the central Head Spearman remains within noise (-0.001): the cap activates symmetrically on the training and generated corpora, so the ratio metric on the shared support cancels. ENZYMES is the only dataset where the cap activates asymmetrically (training side dominated, since the model’s generated sequences are short enough that the cap is not reached on the generated side), producing a $+0.152$ Head Spearman shift driven by 667 training-only Head patterns becoming shared once the guard is removed. We therefore report the no-cap numbers for ENZYMES throughout Figure 2 and the corresponding ENZYMES rows of Table 13, while the four other TU datasets and PCQM4Mv2 remain on the default cap. Our central claims (TU memorization regime,

PCQM4Mv2 decoupling, persistent Tail deficit, cross-serialization agreement) hold under either choice for every dataset. Notably, lifting the cap on ENZYMES eliminates the Head/Torso missing mass while leaving the Tail deficit essentially unchanged (-0.003 on Tail missing mass and ≈ 0 on Tail ρ), which isolates the deficit to rare substructures more cleanly than under the original cap.

For ENZYMES specifically, the no-cap rerun has been propagated to the DFS-canonical main results table, the calibrated baseline, the strata breakdown, the Head–Tail gap, the per-stratum decoding-seed ablation (DFS rows), and the cross-baseline strata diagnostic (Tables 1, 2, 13, 15, 16, and 23), as well as Table 4 (single-seed DGMG calibration). The six-configuration decoding sweep (Table 19), the $\sigma = 0.01$ sensitivity row (Table 17), and the DGMG multi-seed strata and two-way ablation (Tables 14, the DGMG rows of Table 16, and the $s_t = 1337$ DFS column and DGMG rows of Table 24) retain the default cap because the corresponding no-cap reruns either exceed the projection-memory budget ($\sigma = 0.01$) or were deferred for the camera-ready release (DGMG multi-seed). The qualitative Head/Torso/Tail ordering and the Tail-stratum deficit hold under either choice on every dataset, as the symmetry argument and the empirical TU + PCQM4Mv2 audit above establish.

B Proofs of Propositions 1–2 and Corollary 3

Proof of Proposition 1. For any measurable $A \subseteq \bar{\mathcal{G}}$, $\psi_{\#}Q_X(A) = Q_X(\psi^{-1}(A))$ and similarly for $\psi_{\#}P_X$. By the dual characterization $d_{\text{TV}}(\mu, \nu) = \sup_B |\mu(B) - \nu(B)|$, with the supremum over measurable sets,

$$\begin{aligned} d_{\text{TV}}(\psi_{\#}Q_X, \psi_{\#}P_X) &= \sup_A |Q_X(\psi^{-1}(A)) - P_X(\psi^{-1}(A))| \\ &\leq \sup_B |Q_X(B) - P_X(B)| \\ &= d_{\text{TV}}(Q_X, P_X), \end{aligned}$$

since ψ is measurable and $\{\psi^{-1}(A) : A \subseteq \bar{\mathcal{G}} \text{ measurable}\}$ is a sub-family of the measurable sets in \mathcal{X} . This is a special case of the data-processing inequality for total variation. \square

Proof of Proposition 2. For any bounded $f : \bar{\mathcal{G}} \rightarrow \mathbb{R}$,

$$|\mathbb{E}_{Q_G} f - \mathbb{E}_{P_G} f| = \left| \int f d(Q_G - P_G) \right| \leq \|f\|_{\infty} |Q_G - P_G|(\bar{\mathcal{G}}) = 2\|f\|_{\infty} d_{\text{TV}}(Q_G, P_G).$$

Here $|Q_G - P_G|$ denotes the total variation measure of the signed measure $Q_G - P_G$. Combining with Proposition 1 gives the second inequality. \square

Proof of Corollary 3. Take $Q_X^{(\text{mem})}$ to be the empirical replay distribution concentrating on $\{\phi(G_i)\}_{i=1}^n$, so that $Q_G^{(\text{mem})} = \hat{P}_G^{\text{boot}}$. For any $\varepsilon > 0$, let $Q_X^{(\text{gen})}$ be any sequence model satisfying $d_{\text{TV}}(Q_X^{(\text{gen})}, P_X) < \varepsilon/(2\|f\|_{\infty})$ with positive mass outside $\{\phi(G_i)\}$. Proposition 2 then gives $|\mathbb{E}_{Q_G^{(\text{mem})}} f - \mathbb{E}_{Q_G^{(\text{gen})}} f| < \varepsilon$. \square

C Algorithms

This appendix collects the four algorithms referenced in the main text: the canonical DFS code construction underlying our serialization map ϕ ; the bootstrap calibration procedure of §4.3 that realizes \hat{P}_G^{boot} empirically; and the SMILES-to-DFS preprocessing pipeline used for PCQM4Mv2.

Algorithm 1: Canonical DFS code via rightmost-path extension (referenced from §4.1).

Input: labeled graph $G = (V, E, \ell_V, \ell_E)$.

Output: canonical DFS code $C_{\min}(G)$.

$\mathcal{C} \leftarrow \emptyset$;

foreach undirected edge $\{u, v\} \in E$, both directions (u, v) and (v, u) **do**

initialize $C \leftarrow [\langle 0, 1, \ell_V(u), \ell_V(v), \ell_E(u, v) \rangle]$;

$R \leftarrow [u, v]$;

// rightmost path

while any incident edge of G is not yet in C **do**

let r be the last vertex of R ;

if r has an unused edge to an ancestor on R **then**

append the $<_e$ -minimum such backward edge to C ;

else

scan R from right to left and enumerate forward edges (w, x) with $w \in R$ and

$x \notin V(C)$;

append the candidate with smallest label triple $(\ell_V(w), \ell_V(x), \ell_E(w, x))$ and

update R ;

$\mathcal{C} \leftarrow \mathcal{C} \cup \{C\}$;

return $\arg \min_{C \in \mathcal{C}} C$ under lexicographic order on $<_e$;

Algorithm 2: Bootstrap calibration of distributional metrics (referenced from §4.3).

Input: training graphs \mathbf{D}_{tr} , target sample size $n_{\text{gen}} = |\mathbf{D}_{\text{gen}}|$, number of repeats R , gSpan parameters (σ, upper) .

Output: reference samples $\{(\rho^{(r)}, \text{JSD}^{(r)}, \text{MM}^{(r)})\}_{r=1}^R$.

$\mathcal{P}_{\text{tr}}, s_{\text{tr}} \leftarrow \text{gSpan}(\mathbf{D}_{\text{tr}}; \sigma, \text{upper})$;

for $r = 1, \dots, R$ **do**

draw $\mathbf{D}^{(r)} \sim \hat{P}_G^{\text{boot}}$ with $|\mathbf{D}^{(r)}| = n_{\text{gen}}$; // i.i.d. resample from training graphs

$\mathcal{P}^{(r)}, s^{(r)} \leftarrow \text{gSpan}(\mathbf{D}^{(r)}; \sigma, \text{upper})$;

$\rho^{(r)} \leftarrow \text{Spearman}(s_{\text{tr}}, s^{(r)})$ on $\mathcal{P}_{\text{tr}} \cap \mathcal{P}^{(r)}$;

$\text{JSD}^{(r)} \leftarrow \text{JSD}(p_{\text{tr}}, p^{(r)})$, $\text{MM}^{(r)} \leftarrow \sum_{g \in \mathcal{P}_{\text{tr}} \setminus \mathcal{P}^{(r)}} p_{\text{tr}}(g)$;

return $\{(\rho^{(r)}, \text{JSD}^{(r)}, \text{MM}^{(r)})\}_{r=1}^R$;

Algorithm 3: PCQM4Mv2 Preprocessing: SMILES to Canonical DFS Code.

Input: PCQM4Mv2 dataset $\mathcal{D} = \{(s_i, y_i)\}_{i=1}^N$, where s_i is a SMILES string and $y_i \in \mathbb{R}$ is the HOMO-LUMO gap.

Output: Dataset $\mathcal{D}' = \{(c_i, y_i)\}$ of canonical DFS codes with labels.

```
// Phase 1: SMILES to molecular graph
foreach  $(s_i, y_i) \in \mathcal{D}$  (in parallel) do
   $M_i \leftarrow \text{MOLFROMSMILES}(s_i)$ ; // RDKit SMILES parser
  if  $M_i = \emptyset$  then
    discard  $(s_i, y_i)$ ;
    continue;
   $V_i \leftarrow \{(v, \ell_v) \mid v \in M_i, \ell_v = \text{GETSYMBOL}(v)\}$ ;
   $E_i \leftarrow \{(u, v, \ell_e) \mid (u, v) \in M_i, \ell_e = \text{GETBONDTYPE}(u, v)\}$ ;
   $G_i \leftarrow (V_i, E_i)$ ; // Labeled molecular graph
Remove all entries where  $M_i = \emptyset$ ; // Drop NA

// Phase 2: canonical DFS code generation
foreach  $G_i = (V_i, E_i)$  do
   $c^* \leftarrow \infty$ ;
  foreach  $v_0 \in V_i$  do
     $c \leftarrow \text{DFSTRAVERSAL}(G_i, v_0)$ ;
    if  $c < c^*$  (lexicographic order) then
       $c^* \leftarrow c$ ;
   $c_i \leftarrow c^*$ ; // Canonical DFS code
```

Result: $\mathcal{D}' = \{(c_i, y_i)\}$, split into train / valid / test.

Algorithm 4: DFSTRAVERSAL(G, v_0).

Input: Labeled graph $G = (V, E)$, start node v_0 .

Output: DFS code sequence \mathcal{C} .

$\mathcal{C} \leftarrow []$, $visited \leftarrow \emptyset$, $order \leftarrow \{\}$;

Function DFSVisit($v, parent$):

```
   $visited \leftarrow visited \cup \{v\}$ ;
   $order[v] \leftarrow |order|$ ;
  foreach  $u \in \mathcal{N}(v)$  do
    if  $u \notin visited$  then
      // Forward edge
       $\mathcal{C}.\text{append}(\langle order[v], |order|, \ell_v, \ell_u, \ell_{vu}, \text{fwd} \rangle)$ ;
      DFSVisit( $u, v$ );
    else
      if  $u \neq parent$  then
        // Back edge
         $\mathcal{C}.\text{append}(\langle order[v], order[u], \ell_v, \ell_u, \ell_{vu}, \text{bck} \rangle)$ ;
DFSVisit( $v_0, \emptyset$ );
return  $\mathcal{C}$ ;
```

D Calibrated metrics for DGMG serialization

Table 4 reports the bootstrap-calibrated metrics for the DGMG action-sequence serialization, the DGMG counterpart of Table 2 in the main text. The same qualitative pattern holds: in 3 of 5 datasets the model is at or below the bootstrap median ($\Delta\rho \leq 0$ or $z \leq 0$). The exceptions are PROTEINS-DGMG and ENZYMES-DGMG, which sit at the 100th and 80th percentile respectively ($z = +1.49$ and $z = +0.69$). For PROTEINS the bootstrap is the narrowest of the five TU datasets (the corpus is large and bootstrap-resampled ρ already saturates near 0.98), so a $z = +1.49$

deviation translates to $\Delta\rho = +0.009$ in absolute terms—inside the decoding-seed variability documented in Appendix I.4—rather than evidence of meaningfully super-bootstrap structural learning. The ENZYMES–DGMG entry uses the no-cap gBolt rerun (Limitations (g)); under the default cap it sits far below the bootstrap ($\Delta\rho = -0.024$, $z = -4.30$, 0th percentile), so the above-median appearance here is itself a consequence of removing the asymmetric pruning, not of stronger structural learning.

Table 4: Calibrated metrics for DGMG serialization (counterpart of Table 2; single training seed = 42; ENZYMES values are taken from the no-cap gBolt rerun to match the no-cap audit in Limitations (g)).

| Dataset | ρ | $\Delta\rho$ | $z(\rho)$ | Pctile |
|----------|--------|--------------|-----------|--------|
| MUTAG | 0.989 | -0.001 | -0.30 | 30% |
| PTC_MR | 0.986 | +0.008 | +0.89 | 70% |
| ENZYMES | 0.993 | +0.001 | +0.69 | 80% |
| PROTEINS | 0.989 | +0.009 | +1.49 | 100% |
| NCI1 | 0.986 | -0.004 | -1.57 | 10% |

E NLL hit/miss analysis (full)

For each unique training sequence we compute the average per-token negative log-likelihood (NLL) under the trained model, classify sequences as *hits* (reproduced in the generated set) or *misses* (not reproduced), and test whether the NLL distributions differ via the Mann–Whitney U test.

Table 5: NLL analysis (DFS canonical, single training seed = 42). Hit: training sequences reproduced in generation. Miss: not reproduced. MW: Mann–Whitney U test p -value. *: $p < 0.05$; **: $p < 0.01$; ***: $p < 0.001$.

| Dataset | Hit | Miss | NLL _{hit} | NLL _{miss} | MW p |
|----------|-----|------|--------------------|---------------------|--------------------------|
| MUTAG | 169 | 19 | 2.81 | 2.84 | 0.040* |
| PTC_MR | 287 | 51 | 5.40 | 4.98 | 7.3×10^{-4} *** |
| ENZYMES | 429 | 162 | 3.87 | 4.21 | 2.7×10^{-6} *** |
| PROTEINS | 539 | 533 | 3.91 | 3.74 | 0.060 |
| NCI1 | 883 | 3064 | 5.02 | 5.31 | 2.6×10^{-5} *** |

For ENZYMES and NCI1, hits have significantly lower NLL than misses ($p < 10^{-5}$), confirming that the model assigns higher probability to sequences it memorizes. PTC_MR shows an inverted pattern: misses have lower NLL than hits ($p < 0.001$), driven by 98.3% precision where the few misses are short, high-probability sequences not selected during sampling. PROTEINS shows no significant difference ($p = 0.06$) with roughly equal hit and miss counts, suggesting a more uniform probability landscape. The MUTAG entry is reported here at training seed 42; the MUTAG multi-seed aggregate (Appendix O, Table 27) gives Mann–Whitney $p = 0.0753 \pm 0.0113$ across two completed training seeds, consistent with the single-seed reading and with a memorization-dominated regime in which hit and miss training sequences carry essentially the same NLL.

F Decoding factor decomposition (full)

We decompose metric variance into checkpoint (learning) and decoding (inference) effects via a one-way variance decomposition, $\eta_{\text{ckpt}}^2 = \text{Var}_{\text{ckpt}} / (\text{Var}_{\text{ckpt}} + \text{Var}_{\text{decode}})$.

For PTC_MR, ENZYMES, and NCI1, decoding configuration explains 57–71% of Spearman variance: temperature and sampling strategy have a larger effect on distributional alignment than training progress on these datasets. Missing-mass variance is dominated by training progress in most datasets (> 76%), reflecting that longer training reduces pattern omission regardless of decoding strategy. Novelty is almost entirely determined by decoding (73–99% for PTC_MR, ENZYMES, PROTEINS), confirming that exploration of the generation space is an inference-time phenomenon.

Table 6: Factor effect ratios (η^2 ; single training seed = 42). Values indicate the fraction of metric variance attributable to each factor.

| Dataset | Spearman ρ | | Missing Mass | | Novel Mass | |
|----------|-----------------|--------|--------------|--------|------------|--------|
| | Ckpt | Decode | Ckpt | Decode | Ckpt | Decode |
| MUTAG | 0.87 | 0.13 | 0.99 | 0.01 | 0.60 | 0.40 |
| PTC_MR | 0.29 | 0.71 | 0.50 | 0.50 | 0.27 | 0.73 |
| ENZYMES | 0.37 | 0.63 | 0.89 | 0.11 | 0.01 | 0.99 |
| NCI1 | 0.43 | 0.57 | 0.55 | 0.45 | 0.45 | 0.55 |
| PROTEINS | 0.75 | 0.25 | 0.76 | 0.24 | 0.13 | 0.87 |

Implication for calibrated evaluation. The combination of these η^2 values and the per-config sweep in Table 19 carries a methodological consequence for the calibrated diagnostic. The intra-dataset spread induced by decoding alone is large enough to flip the verdict that the bootstrap-calibrated comparison of §6 (Calibrated baseline comparison) returns: e.g. on MUTAG the same checkpoint moves from $\rho = 0.989$ under `topk_only` to $\rho = 0.639$ under `tp_high`, spanning the entire bootstrap percentile range. A single decoding choice therefore underdetermines the memorization–alignment position; we report `both_default` in the main text for comparability with prior work and document the full sweep here so that the diagnostic can be re-evaluated under any other choice.

G Aggregate whole-graph statistic MMD (full)

Table 7 reports the four classical whole-graph statistic MMDs (degree, clustering, orbit, spectral) under DFS canonical `both_default` decoding for every TU benchmark. All values sit in $\leq 0.6 \times 10^{-3}$, i.e. below standard reporting thresholds in graph-generation papers; the discussion below explains why this is uninformative in the present regime.

Table 7: Whole-graph statistic MMD metrics (DFS canonical, `both_default`, single training seed = 42). All values $\times 10^3$.

| Dataset | Degree | Clustering | Orbit | Spectral |
|----------|--------|------------|-------|----------|
| MUTAG | 0.15 | 0.38 | 0.22 | 0.41 |
| PTC_MR | 0.04 | 0.01 | 0.16 | 0.36 |
| ENZYMES | 0.28 | 0.52 | 0.35 | 0.48 |
| PROTEINS | 0.24 | 0.45 | 0.30 | 0.52 |
| NCI1 | 0.08 | 0.12 | 0.10 | 0.25 |

These low values are consistent with high memorization: if most generated graphs are exact copies of training graphs, their aggregate statistics will trivially match training statistics regardless of any structural learning.

Cross-model MMD on TU. Table 8 extends the LLM-DFS numbers above with the three structural baselines used in §6 (Structural baselines), averaged across the five TU benchmarks. Both unlabeled baselines (GraphRNN and DGMG-official) pass the label-agnostic deg/orb checks but fail WL by $\sim 10^2\times$, exposing the labeled-structure failure that label-free MMD hides.

H Robustness across serializations: WL-kernel and DGMG memorization

Per-dataset graph statistics. Table 9 reports the per-graph statistics of the six benchmarks evaluated in this paper. The TU benchmarks span 188–4,110 graphs with average $|V| \in [14, 39]$, while PCQM4Mv2 contributes 3.75M graphs at average $|V| = 14.1$, giving roughly four orders of magnitude of corpus-size separation between TU and PCQM4Mv2 at comparable per-graph size.

Table 8: Cross-model whole-graph statistic MMD on TU (mean over five benchmarks, single training seed = 42 for LLM-DFS/DGMG; per-dataset values in Appendix N). deg/orb $\times 10^{-3}$, WL raw. GraphRNN/DGMG-official pass the label-agnostic deg/orb checks yet fail WL by $\sim 10^2\times$, exposing structural failure that label-free MMD hides.

| Model | deg ($\times 10^{-3}$) | orb ($\times 10^{-3}$) | WL |
|---------------|--------------------------|--------------------------|--------|
| GraphRNN | 0.11 | 0.08 | 0.753 |
| DGMG-official | 2.56 | 2.95 | 0.770 |
| DiGress | 2.07 | 16.52 | 0.026 |
| LLM-DFS | 0.16 | 0.23 | <0.001 |

Table 9: Graph-level dataset statistics. PCQM4Mv2 numbers are reported from OGB-LSC [Hu et al., 2021]; we use the canonical-DFS training split, which contains 3,371,958 sequences (3,104,677 unique).

| Dataset | $ G $ | Avg $ V $ | Avg $ E $ | Max $ V $ | Avg Deg | Density |
|----------|-----------|-----------|-----------|-----------|---------|---------|
| MUTAG | 188 | 17.9 | 19.8 | 28 | 2.19 | 0.138 |
| PTC_MR | 344 | 14.3 | 14.7 | 64 | 1.98 | 0.214 |
| ENZYMES | 600 | 32.6 | 62.1 | 126 | 3.86 | 0.160 |
| PROTEINS | 1,113 | 39.1 | 72.8 | 620 | 3.73 | 0.212 |
| NCI1 | 4,110 | 29.9 | 32.3 | 111 | 2.16 | 0.089 |
| PCQM4Mv2 | 3,746,620 | 14.1 | 14.6 | 53 | 2.07 | 0.147 |

Cross-serialization robustness. We compare canonical DFS code and DGMG action sequences using format-agnostic WL-kernel metrics (Table 11). WL-MMD values stay below 0.006 and coverage above 0.92 for every dataset under both serializations, indicating that the two formats produce graph distributions of comparable distance to the training set in this metric. Using a whole-graph memorization detector, DGMG memorization is at least as high as DFS in every dataset (Table 12); memorization is therefore not specific to DFS-code serialization. The frequency-stratified pattern of §6 (Frequency-stratified analysis) is also reproduced under DGMG (Table 14 below): we treat this as robustness evidence rather than a serialization-invariance claim, since the two canonicalizations remain a small slice of the possible serializations and the contrast is restricted to what these formats expose to gSpan.

Table 10: Serialized-sequence statistics. “Mean / Max L ” is the sequence length in tokens after subword tokenization, excluding BOS/EOS. “ $|V_{\text{tok}}|$ ” is the vocabulary size of the serialization-specific tokenizer, excluding the four special tokens $\langle s \rangle$, $\langle \text{unk} \rangle$, $\langle \text{pad} \rangle$, $\langle \text{mask} \rangle$. PCQM4Mv2 length statistics are estimated on a uniformly random subsample of 5×10^4 training graphs (vocabulary sizes are exact). Canonical DFS encodes one event (v / e) per token over a combinatorial node \times edge-label vocabulary, while DGMG factorizes each event into single-symbol actions (ADD_NODE, ADD_EDGE, TARGET, ...) over a tiny vocabulary; this is why DGMG sequences are several times longer but use far fewer unique tokens.

| Dataset | Canonical DFS | | | DGMG | | |
|----------|---------------|---------|--------------------|----------|---------|--------------------|
| | Mean L | Max L | $ V_{\text{tok}} $ | Mean L | Max L | $ V_{\text{tok}} $ |
| MUTAG | 19.8 | 33 | 382 | 78.4 | 125 | 39 |
| PTC_MR | 14.7 | 71 | 1,257 | 61.0 | 273 | 84 |
| ENZYMES | 60.8 | 149 | 5,737 | 192.5 | 545 | 129 |
| PROTEINS | 69.1 | 1,049 | 18,133 | 226.7 | 3,341 | 568 |
| NCI1 | 31.2 | 108 | 6,766 | 127.3 | 463 | 148 |
| PCQM4Mv2 | 16.0 | 49 | 12,293 | 60.4 | 171 | 83 |

Table 11: WL kernel metrics by serialization format (single training seed = 42). WL-MMD: Weisfeiler–Lehman maximum mean discrepancy (\downarrow). Cov: fraction of training graphs “covered” by the generated set (\uparrow). Div: mean pairwise dissimilarity among generated graphs (\uparrow).

| Dataset | WL-MMD (\downarrow) | | Coverage (\uparrow) | | Diversity (\uparrow) | |
|----------|-------------------------|--------|-------------------------|-------|--------------------------|-------|
| | DFS | DGMG | DFS | DGMG | DFS | DGMG |
| MUTAG | -0.001 | -0.001 | 0.995 | 0.989 | 0.720 | 0.712 |
| ENZYMES | 0.002 | 0.001 | 0.960 | 0.970 | 0.630 | 0.628 |
| NCII | 0.000 | 0.000 | 0.926 | 0.942 | 0.698 | 0.700 |
| PROTEINS | 0.001 | 0.006 | 0.973 | 0.946 | 0.544 | 0.570 |
| PTC_MR | -0.001 | -0.002 | 0.980 | 0.986 | 0.452 | 0.427 |

Table 12: DGMG memorization rates under whole-graph matching (single training seed = 42). DGMG Precision: fraction of generated DGMG sequences whose decoded graph is isomorphic to a training graph. DFS Precision is the EM of Eq. (1) reproduced from Table 1 for comparison.

| Dataset | DGMG Precision | DFS Precision |
|----------|----------------|---------------|
| MUTAG | 100.0% | 82.8% |
| PTC_MR | 99.4% | 98.3% |
| ENZYMES | 98.9% | 97.5% |
| PROTEINS | 91.8% | 89.1% |
| NCII | 100.0% | 100.0% |

I Frequency-Stratified Diagnostics: Full Results

This appendix consolidates all per-stratum numerical results that the main-text figure-only frequency-stratified analysis (§6) draws on. We present them in four subsections that share a common structure: the DFS-canonical Head/Torso/Tail breakdown (§I.1), its DGMG-serialization counterpart (§I.2), the Head–Tail gap and Tail-coverage rate derived from the DFS table (§I.3), and the $n = 5$ decoding-seed ablation that supplies the \pm std values of both stratified tables (§I.4).

I.1 DFS canonical

Table 13 gives the numeric DFS-canonical Head/Torso/Tail breakdown underlying Figure 2. The table is here rather than in the main text so that the body text can focus on the visual frequency-stratified pattern while preserving exact per-dataset values for comparison and reproducibility.

Table 13: Frequency-stratified metrics (DFS canonical, single training seed = 42), mean \pm std over $n = 5$ decoding-seed reruns. Missing: fraction of stratum support mass absent in generated set. “ ρ ” is the intersection Spearman; trainkeys- ρ (penalizing omitted patterns) is reported alongside in Appendix I.4.

| Dataset | Missing Mass | | | Spearman ρ | | |
|----------|--------------|-------|-------------------|-----------------|-------|-------------------|
| | Head | Torso | Tail | Head | Torso | Tail |
| MUTAG | 0.000 | 0.003 | 0.135 \pm 0.099 | 0.911 | 0.986 | 0.420 \pm 0.296 |
| PTC_MR | 0.000 | 0.008 | 0.220 \pm 0.145 | 0.998 | 0.975 | 0.562 \pm 0.456 |
| ENZYMES | 0.000 | 0.001 | 0.132 \pm 0.076 | 0.940 | 0.981 | 0.283 \pm 0.059 |
| PROTEINS | 0.000 | 0.002 | 0.159 \pm 0.056 | 0.959 | 0.974 | 0.258 \pm 0.040 |
| NCII | 0.000 | 0.001 | 0.199 \pm 0.075 | 0.988 | 0.987 | 0.350 \pm 0.111 |

I.2 DGMG action sequences

Table 14 reproduces the Head/Torso/Tail breakdown of the main-text frequency-stratified analysis (§6) under DGMG action-sequence serialization, mirroring the decoding-seed averaging used for

DFS canonical (mean \pm std over $n = 5$ reruns of the same LLaMA-SMALL checkpoint). The Head–Tail asymmetry is qualitatively the same as under DFS canonical (Table 13): Head and Torso ρ exceed 0.91 and 0.97 on every dataset, while seed-mean Tail ρ ranges 0.23–0.41 with Tail missing mass between 15% and 39%. Decoding-stage variance is again concentrated on Tail (Tail ρ std up to 0.46 on MUTAG/PTC_MR; Tail miss std up to 0.18), consistent with the canonical observation that 1024 samples are too few to densely cover the bottom-decile pattern set on small TU benchmarks.

Table 14: Frequency-stratified metrics (DGMG serialization, single training seed = 42), mean \pm std over $n = 5$ decoding-seed reruns. “ ρ ” is the intersection Spearman; trainkeys- ρ in Appendix I.4. ENZYMES values retain the default cap=500K; the no-cap DGMG multi-seed audit is deferred to the camera-ready—see Limitations (g).

| Dataset | Missing Mass | | | Spearman ρ | | |
|----------|--------------|-------|-------------------|-----------------|-------|-------------------|
| | Head | Torso | Tail | Head | Torso | Tail |
| MUTAG | 0.000 | 0.003 | 0.389 \pm 0.181 | 0.913 | 0.979 | 0.231 \pm 0.462 |
| PTC_MR | 0.000 | 0.005 | 0.177 \pm 0.119 | 0.999 | 0.975 | 0.406 \pm 0.328 |
| ENZYMES | 0.039 | 0.006 | 0.150 \pm 0.105 | 0.981 | 0.990 | 0.379 \pm 0.049 |
| PROTEINS | 0.000 | 0.005 | 0.261 \pm 0.102 | 0.928 | 0.970 | 0.265 \pm 0.028 |
| NCII | 0.000 | 0.001 | 0.163 \pm 0.093 | 0.958 | 0.978 | 0.296 \pm 0.031 |

DGMG shows a similar Head–Tail gap to DFS canonical, providing robustness evidence across the two serializations studied. Comparing seed-averaged Tail ρ side-by-side under decoding-seed averaging ($n = 5$ each), the per-dataset ordering is mixed and within overlapping decoding-seed CIs in three of five cases: DGMG seed-mean is higher on ENZYMES (0.38 vs. DFS 0.28) and PROTEINS (0.27 vs. 0.26, essentially equal), roughly matched on PTC_MR (DGMG 0.41 \pm 0.33 vs. DFS 0.56 \pm 0.46, both with very wide CIs driven by the \sim 15 shared tail patterns), and lower on MUTAG (0.23 vs. 0.42) and NCII (0.30 vs. 0.35). The qualitative Head–Tail gap is preserved under both formats—supporting expectation (E4) of cross-serialization robustness—while the per-dataset reordering appears to reflect serialization-specific tail-coverage biases plus substantial decoding-stage noise rather than a systematic advantage of either tokenization.

I.3 Head–Tail gap and Tail Coverage Rate

Head–Tail gap. Table 15 summarizes the Head–Tail gap $\Delta\rho = \rho_{\text{head}} - \rho_{\text{tail}}$ alongside the stratum missing-mass values, with ρ_{tail} averaged over $n = 5$ decoding-seed reruns. The rank-correlation gap is large on every TU dataset ($\Delta\rho = 0.44$ –0.70): the model preserves rank ordering for high-frequency patterns but loses it sharply on rare patterns, even when only the patterns it does generate are ranked. The missing-mass deficit is concentrated in the Tail stratum (0.132–0.220 vs. ≤ 0.008 for Head/Torso), confirming that the Head–Tail asymmetry is driven by Tail under-coverage rather than uniformly distributed errors.

Table 15: Head–Tail gap analysis derived from Table 13 (single training seed = 42). $\Delta\rho$: Head ρ minus Tail ρ ; larger values indicate greater frequency dependence.

| Dataset | ρ_{head} | ρ_{tail} | $\Delta\rho$ | Miss _{head} | Miss _{tail} |
|----------|----------------------|----------------------|--------------|----------------------|----------------------|
| MUTAG | 0.911 | 0.420 | 0.491 | 0.000 | 0.135 |
| PTC_MR | 0.998 | 0.562 | 0.436 | 0.000 | 0.220 |
| ENZYMES | 0.940 | 0.283 | 0.657 | 0.000 | 0.132 |
| PROTEINS | 0.959 | 0.258 | 0.701 | 0.000 | 0.159 |
| NCII | 0.988 | 0.350 | 0.638 | 0.000 | 0.199 |

Tail Coverage Rate (TCR). $\text{TCR} = |\mathcal{P}_{\text{tail}}^{\text{shared}}| / |\mathcal{P}_{\text{tail}}^{\text{train}}|$ is the fraction of tail patterns that appear at least once in the generated set. Across the TU runs, TCR remains below one in every dataset–serialization condition, confirming that the Tail deficit includes complete omission of rare patterns rather than only support underestimation.

I.4 Decoding-seed ablation

The TU strata estimates of Table 13 are sensitive to the random sampling at decoding time. For each TU dataset and the LLaMA-SMALL (132M) checkpoint we re-evaluated the `both_default` configuration ($T = 1.0$, $\text{top-}p = 0.95$, $\text{top-}k = 50$, 1024 samples) under five fixed `torch.manual_seed` values $s \in \{0, 1, 2, 3, 4\}$. Generation, gSpan mining, and frequency-stratified analysis were otherwise identical to the main pipeline; bootstrap, kernel, MMD, and NLL stages were skipped to keep the ablation tractable on CPU.

Table 16 reports the per-stratum mean and sample standard deviation across the five seeds. The Head and Torso strata are highly stable ($\text{std} \leq 0.014$ for ρ , ≤ 0.019 for missing mass on every dataset). Tail estimates are markedly noisier: intersection ρ swings by $\text{std } 0.040\text{--}0.456$ across reruns of the same checkpoint, and Tail missing mass by $0.056\text{--}0.145$. The trainkeys variant (which fills omitted patterns with zero before ranking) is consistently more stable than intersection: standard deviations are typically $1.5\text{--}5\times$ smaller, and the gap between the two metrics is largest on datasets with few tail patterns (PTC_MR has only 12–20 shared tail patterns per draw, making intersection-based rank correlation highly contingent on which exact patterns are generated). We therefore recommend reading the trainkeys ρ column as the more reliable Tail-rank summary.

Table 16: Per-stratum decoding-seed ablation ($n = 5$ reruns of the same LLaMA-SMALL checkpoint with `torch.manual_seed` $\in \{0, 1, 2, 3, 4\}$). Top: DFS canonical. Bottom: DGMG action sequences (with `max_length=512`). Values are mean \pm sample std. “ ρ_{\cap} ” is intersection Spearman (only patterns shared between train and generation are ranked); “ ρ_{tk} ” is trainkeys Spearman (full train support, with `generated=0` for missing patterns). DFS ENZYMES uses the no-cap gBolt rerun; DGMG ENZYMES retains the default `cap=500K` because the no-cap DGMG multi-seed rerun is deferred to the camera-ready—see Limitations (g).

| Dataset | Tail miss | Tail ρ_{\cap} | Tail ρ_{tk} | Head ρ_{\cap} | Torso ρ_{\cap} |
|-----------------------------|-------------------|--------------------|-------------------|--------------------|---------------------|
| <i>DFS canonical</i> | | | | | |
| MUTAG | 0.135 \pm 0.099 | 0.420 \pm 0.296 | 0.609 \pm 0.108 | 0.911 | 0.986 |
| PTC_MR | 0.220 \pm 0.145 | 0.562 \pm 0.456 | 0.560 \pm 0.418 | 0.998 | 0.975 |
| ENZYMES | 0.132 \pm 0.076 | 0.283 \pm 0.059 | 0.325 \pm 0.049 | 0.940 | 0.981 |
| PROTEINS | 0.159 \pm 0.056 | 0.258 \pm 0.040 | 0.311 \pm 0.038 | 0.959 | 0.974 |
| NCII | 0.199 \pm 0.075 | 0.350 \pm 0.111 | 0.380 \pm 0.094 | 0.988 | 0.987 |
| <i>DGMG action sequence</i> | | | | | |
| MUTAG | 0.389 \pm 0.181 | 0.231 \pm 0.462 | 0.457 \pm 0.145 | 0.913 | 0.979 |
| PTC_MR | 0.177 \pm 0.119 | 0.406 \pm 0.328 | 0.412 \pm 0.374 | 0.999 | 0.975 |
| ENZYMES | 0.150 \pm 0.105 | 0.379 \pm 0.049 | 0.430 \pm 0.024 | 0.981 | 0.990 |
| PROTEINS | 0.261 \pm 0.102 | 0.265 \pm 0.028 | 0.321 \pm 0.030 | 0.928 | 0.970 |
| NCII | 0.163 \pm 0.093 | 0.296 \pm 0.031 | 0.310 \pm 0.044 | 0.958 | 0.978 |

Implication for single-draw reporting. Earlier single-draw values (e.g. MUTAG Tail miss = 0.501, $\rho_{\cap} = 0.820$ from one decoding lottery in the original seed-42 eval) sit outside the $n = 5$ mean by $> 3\sigma$ on Tail miss and indicate that 1024 samples are not sufficient to densely cover the bottom-decile pattern set on small TU benchmarks. The seed-averaged values reported in Table 13 attenuate this by reporting mean \pm std, but the residual standard deviations remain substantial—especially on PTC_MR, where the tail support set is so sparse (~ 15 patterns) that rank correlation is intrinsically contingent on the realized draw. We treat the Tail ρ column on TU as a noisy diagnostic and read it together with Tail missing mass, which is more stable. The same caveat does not apply to PCQM4Mv2 (Appendix P), where the $\sim 10,000$ -pattern reference set absorbs most of the sample-level noise and the per-seed mean \pm half-width over the 5-subsample bootstrap is included in the table.

Cross-training-seed extension. The same five-decoding-seed ablation has also been run on the seed-1337 training checkpoint for every TU dataset and serialization, giving a full 2×5 training-seed \times decoding-seed grid per cell (100 evaluations total). Per-cell training-seed shifts on the decoding-mean are reported in Table 24 and are $|\text{mean}_{42} - \text{mean}_{1337}| \leq 0.05$ on Tail miss and ≤ 0.10 on Tail ρ_{\cap} , all inside the corresponding decoding-seed std bands above. We retain the seed-42 row in

Table 16 as the reference because it matches the checkpoint that supplies the main-text Tables 4 and 22 and Figure 2; the seed-1337 counterpart is the right column of Table 24.

J gSpan Minimum Support Sensitivity

Table 17 contrasts $\sigma = 0.1$ (the main-text default) with the more permissive $\sigma = 0.01$ on three TU datasets (MUTAG, ENZYMES, NCI1). Lowering σ exposes more low-support patterns but leaves the qualitative conclusions (strong head alignment, degraded tail) intact, as discussed below.

Table 17: Effect of gSpan minimum support ratio on key metrics (DFS canonical, single training seed = 42; ENZYMES $\sigma = 0.1$ values use the no-cap gBolt rerun, while $\sigma = 0.01$ retains the default cap=500K because the no-cap mining at $\sigma = 0.01$ exceeds the projection-memory budget on ENZYMES—see Limitations (g)).

| Dataset | Spearman ρ | | JSD | |
|---------|-----------------|---------------|--------------|---------------|
| | $\sigma=0.1$ | $\sigma=0.01$ | $\sigma=0.1$ | $\sigma=0.01$ |
| MUTAG | 0.976 | 0.888 | 0.035 | 0.038 |
| ENZYMES | 0.987 | 0.922 | 0.014 | 0.026 |
| NCI1 | 0.990 | 0.953 | 0.010 | 0.011 |

Lowering the minimum support from 0.1 to 0.01 reduces Spearman ρ (by 0.02–0.09) and marginally increases JSD. This is expected: a lower threshold exposes more tail patterns, where the model performs poorly. The qualitative conclusion—high head alignment, degraded tail performance—remains unchanged.

K Per-Pattern Support Scatter (All Five TU Datasets)

Figure 4 renders the per-pattern alignment underlying the aggregate Spearman ρ for every TU benchmark using the canonical-DFS LLM final eval. Across all five datasets, shared patterns concentrate tightly along the $y = x$ diagonal across several decades of support; train-only and gen-only stripes are thinner for the larger corpora (NCI1, PROTEINS), where the model has more opportunities to recover low-support training motifs.

The PCQM4Mv2 capacity sweep yields the same diagnostic at large scale (Figure 5). Each panel renders subsample 0 of the canonical-DFS LLM, with 1024 generated graphs evaluated against a fixed 10,000-graph training subsample ($\sigma = 0.1$, upper = 8); supports are normalized by the respective sample sizes so the diagonal $y = x$ is comparable across panels. Shared-pattern counts are stable across capacities (244–250) and the dominant deviation from the diagonal is the *gen-only* stripe (71–84 patterns), consistent with the Tail-stratum analysis of the main-text PCQM4Mv2 scaling (§6): the LLM produces unseen patterns of comparable mass to the omitted training tail.

L Full Decoding Sweep Results

This section reports the per-dataset, per-config decoding sweep backing the variance-decomposition statement in the main text. Table 18 lists the six decoding configurations (`both_default`, `nucleus_only`, `topk_only`, `pure_sample`, `tp_high`, `tp_low`) that sweep temperature, top- p , and top- k . Table 19 then reports every metric across all five TU datasets and all six configurations under DFS canonical serialization. The dominant takeaway is that ρ and missing mass shift substantially with the decoding choice (e.g. MUTAG ρ : 0.639 at `tp_high` vs. 0.989 at `topk_only`), so single-config readings overstate the model’s intrinsic capability.

M Checkpoint Trajectories

This appendix combines the MUTAG illustrative table (§M.1) and the per-dataset trajectory figure (§M.2) that consolidates the same diagnostic across all five TU benchmarks under both serializations.

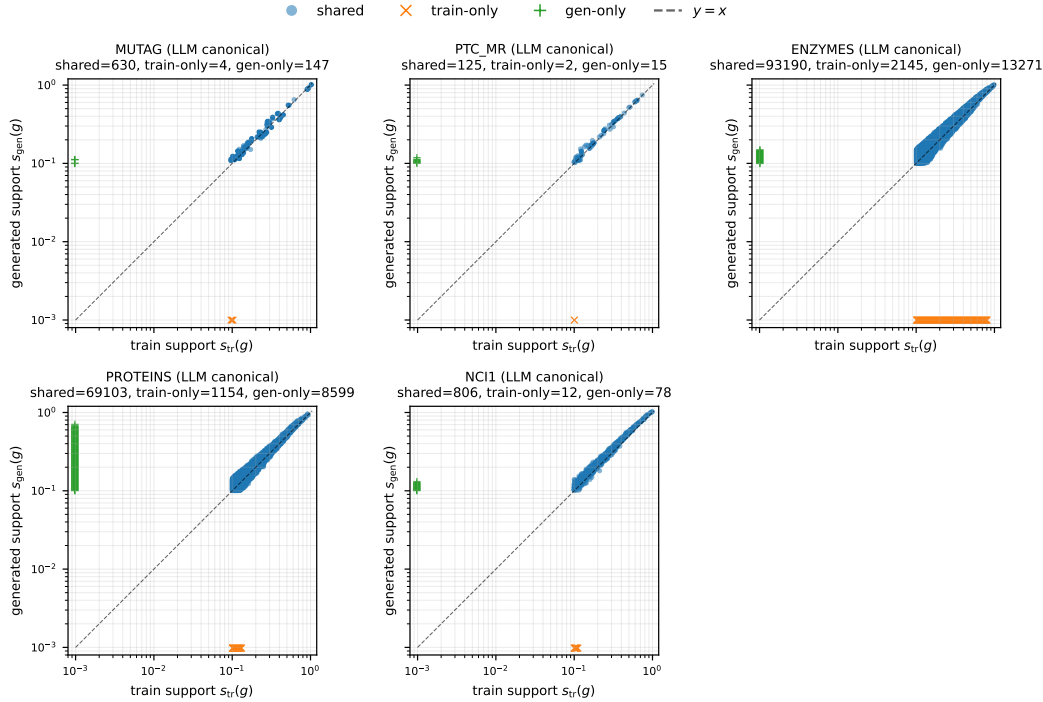


Figure 4: Per-pattern train-vs-generated support on log-log axes for all five TU benchmarks. Blue dots: patterns shared by \mathcal{P}_{tr} and \mathcal{P}_{gen} . Orange \times (placed at $s_{gen} = 10^{-3}$): train-only patterns. Green $+$ (at $s_{tr} = 10^{-3}$): gen-only patterns. The dashed line is $y = x$. All panels use the canonical-DFS LLM final eval (both_default decoding); counts are reported per panel.

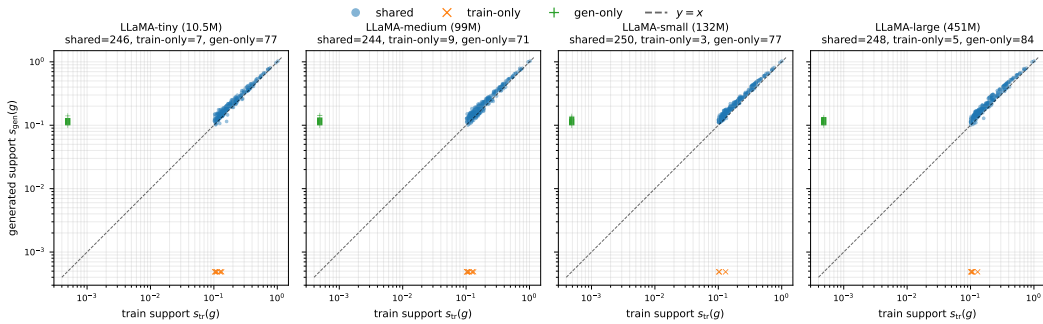


Figure 5: Per-pattern train-vs-generated support on log-log axes for PCQM4Mv2 across the four LLaMA capacities (tiny / medium / small / large) used in the main-text PCQM4Mv2 scaling (§6). Markers as in Figure 4; supports are normalized by sample size (10,000 for train, 1024 for generation) so the diagonal is comparable. Counts of shared / train-only / gen-only patterns are reported per panel.

M.1 MUTAG DFS canonical (illustrative)

Table 20 traces the MUTAG DFS-canonical run across six training checkpoints (steps 600–12000). Spearman ρ climbs $0.18 \rightarrow 0.55 \rightarrow 0.89 \rightarrow 0.98$ in lockstep with precision ($0.001 \rightarrow 0.031 \rightarrow 0.180 \rightarrow 0.645$), while novelty and the unique rate decay symmetrically—i.e. distributional alignment is acquired *simultaneously* with memorization rather than after it, which is the single-dataset evidence behind the “synchronization” claim of Appendix Q.

Table 18: Decoding configurations explored on every TU dataset (`both_default` is the default reported in the main text).

| Config | Description | Temp | top- p | top- k |
|---------------------------|-------------------|------|----------|----------|
| <code>both_default</code> | Standard | 1.0 | 0.95 | 50 |
| <code>nucleus_only</code> | Nucleus sampling | 1.0 | 0.95 | — |
| <code>topk_only</code> | Top- k sampling | 1.0 | — | 50 |
| <code>pure_sample</code> | Unconstrained | 1.0 | — | — |
| <code>tp_high</code> | High temperature | 1.2 | 0.95 | 50 |
| <code>tp_low</code> | Low temperature | 0.8 | 0.95 | 50 |

M.2 Per-Dataset Checkpoint Trajectories

Figure 6 consolidates the per-checkpoint Spearman ρ and Jensen–Shannon divergence trajectories for all five TU datasets in both DFS canonical and DGMG action serializations on a common grid. The MUTAG-DFS panel reproduces the trajectory of Appendix M.1 for visual comparison; the remaining nine combinations are new. Across all ten panels, ρ rises rapidly and saturates near 0.95–0.99 while JSD decays correspondingly, mirroring the random \rightarrow rapid memorization \rightarrow saturation pattern of Appendix Q; ρ never rises without a simultaneous JSD decrease. The raw per-checkpoint values for each panel (including the unique-rate and precision columns omitted from the figure) are produced by the same evaluation pipeline as the main text and are available alongside the LaTeX sources.

N Structural Baselines: DiGress, GraphRNN, DGMG-official

Cross-model comparison (full). Table 21 reports per-dataset memorization, novelty, Spearman ρ , and JSD for the four-model comparison summarized in §6 (Structural baselines). GraphRNN is unlabeled and yields no support overlap on the larger TU datasets, so ρ is undefined there.

Structural-MMD breakdowns. The tables below reproduce the cross-baseline comparison together with structural-MMD breakdowns that are independent of vertex/edge labels. This view locates GraphRNN and DGMG-official—which do not emit labeled graphs and therefore have no shared gSpan support with the labeled training set—on the structural similarity axis.

Frequency-stratified comparison. The Head–Tail asymmetry of the main-text frequency-stratified analysis (§6) is not LLM-specific: every baseline shows a frequency-dependent failure mode of its own (Table 23). DiGress, the only other label-aware baseline, leaves Head perfectly covered (Head miss = 0 in every dataset) but loses 25–72% of Tail mass and yields non-positive Tail ρ_{\cap} on 4 of 5 datasets—larger Tail coverage gaps than LLM-DFS by a factor of 2–5 \times and lower-or-flipped Tail rank correlation. The label-unaware baselines (GraphRNN, DGMG-official) emit unlabeled graphs and therefore share essentially no labeled gSpan support with the training set on 4 of 5 datasets (Head/Torso/Tail miss \approx 1, ρ_{\cap} undefined when the shared-pattern set is empty); MUTAG is the lone exception, whose 7-symbol node vocabulary admits coincidental label coincidence even from unlabeled samples. The strata diagnostic therefore (a) confirms that the LLM-DFS Tail deficit is real, but (b) places it in a regime that all four baselines fail *worse*—so the diagnostic discriminates among graph generators rather than reflecting an LLM-specific bias.

O Multi-Seed Reproducibility

The reproducibility statement (§7) targets mean \pm 95% Student- t CI over three training seeds (`{42, 1337, 2024}`) for every TU result. At submission time, all five TU datasets have completed $n = 2$ training seeds (`{42, 1337}`) under both DFS canonical and DGMG action serializations; seed 2024 is queued and will be added in the camera-ready without further structural changes.

Cross-dataset Tail summary (training-seed \times decoding-seed). Single-decoding-draw aggregation across two training seeds is heavily contaminated by decoding-stage noise: e.g. on MUTAG

Table 19: Complete decoding sweep results for all datasets (DFS canonical, single training seed = 42; MUTAG multi-seed aggregate in Table 25; ENZYMES rows are reported under the default cap=500K for internal consistency across the six decoding configurations, while Table 1 reports the no-cap value of both_default—see Limitations (g)).

| Dataset | Config | Unique | Precision | Novelty | ρ | JSD | Missing |
|----------|--------------|--------|-----------|---------|--------|-------|---------|
| MUTAG | both_default | 0.199 | 0.828 | 0.172 | 0.976 | 0.035 | 0.014 |
| | nucleus_only | 0.512 | 0.336 | 0.664 | 0.945 | 0.032 | 0.017 |
| | topk_only | 0.377 | 0.477 | 0.523 | 0.989 | 0.021 | 0.028 |
| | pure_sample | 0.723 | 0.219 | 0.781 | 0.883 | 0.056 | 0.040 |
| | tp_high | 0.937 | 0.107 | 0.893 | 0.639 | 0.428 | 0.057 |
| | tp_low | 0.128 | 0.947 | 0.053 | 0.938 | 0.049 | 0.016 |
| ENZYMES | both_default | 0.430 | 0.975 | 0.025 | 0.939 | 0.019 | 0.027 |
| | nucleus_only | 0.638 | 0.557 | 0.443 | 0.922 | 0.025 | 0.033 |
| | topk_only | 0.646 | 0.635 | 0.365 | 0.965 | 0.015 | 0.032 |
| | pure_sample | 0.868 | 0.306 | 0.694 | 0.881 | 0.045 | 0.086 |
| | tp_high | 0.977 | 0.055 | 0.945 | 0.452 | 0.345 | 0.266 |
| | tp_low | 0.227 | 1.000 | 0.000 | 0.784 | 0.072 | 0.063 |
| NCI1 | both_default | 0.862 | 1.000 | 0.000 | 0.990 | 0.010 | 0.006 |
| | nucleus_only | 0.849 | 1.000 | 0.000 | 0.984 | 0.013 | 0.007 |
| | topk_only | 0.873 | 0.959 | 0.041 | 0.991 | 0.007 | 0.013 |
| | pure_sample | 0.871 | 0.970 | 0.030 | 0.991 | 0.009 | 0.011 |
| | tp_high | 0.871 | 0.945 | 0.055 | 0.969 | 0.017 | 0.026 |
| | tp_low | 0.690 | 1.000 | 0.000 | 0.915 | 0.040 | 0.025 |
| PROTEINS | both_default | 0.591 | 0.891 | 0.109 | 0.988 | 0.022 | 0.005 |
| | nucleus_only | 0.594 | 0.875 | 0.125 | 0.986 | 0.022 | 0.008 |
| | topk_only | 0.697 | 0.761 | 0.239 | 0.982 | 0.026 | 0.035 |
| | pure_sample | 0.760 | 0.631 | 0.369 | 0.983 | 0.025 | 0.044 |
| | tp_high | 0.900 | 0.332 | 0.668 | 0.868 | 0.161 | 0.363 |
| | tp_low | 0.300 | 0.850 | 0.150 | 0.789 | 0.084 | 0.058 |
| PTC_MR | both_default | 0.285 | 0.983 | 0.017 | 0.950 | 0.063 | 0.007 |
| | nucleus_only | 0.548 | 0.512 | 0.488 | 0.935 | 0.030 | 0.058 |
| | topk_only | 0.438 | 0.701 | 0.299 | 0.947 | 0.032 | 0.043 |
| | pure_sample | 0.713 | 0.358 | 0.643 | 0.925 | 0.068 | 0.133 |
| | tp_high | 0.938 | 0.123 | 0.877 | 0.668 | 0.222 | 0.268 |
| | tp_low | 0.213 | 1.000 | 0.000 | 0.933 | 0.118 | 0.004 |

canonical the seed-42 single draw gives Tail miss 0.501 while the seed-1337 single draw gives 0.032, a swing of 0.47. To disentangle training-seed and decoding-seed effects we ran a full two-way ablation: for each (training seed, dataset, serialization) we re-evaluated the same checkpoint under five fixed `torch.manual_seed` values $\{0, 1, 2, 3, 4\}$. Table 24 reports the resulting decoding-seed mean \pm sample std for both training seeds. *The training-seed shift on the decoding-mean is small: across all 10 TU dataset/serialization cells, the gap $|mean_{42} - mean_{1337}|$ is at most 0.10 for Tail ρ_{\cap} and at most 0.05 for Tail miss, and sits inside the decoding-seed std band on every cell.* Decoding-stage noise therefore dominates training-seed noise for Tail-stratum estimates on TU—the empirical reason we report decoding-seed averages throughout the paper and treat the seed-2024 camera-ready run as a confirmation rather than a load-bearing addition.

Pooled summary (training + decoding, $n=10$). Pooling decoding draws across both training seeds gives a single $n=10$ estimate per cell: Tail miss 0.135–0.430, Tail ρ_{\cap} 0.20–0.60, Tail ρ_{tk} 0.30–0.60, with sample std typically within $1.05\text{--}1.10\times$ the per-training-seed std (i.e. very little additional spread beyond decoding-stage noise alone). This pooled view is the most defensible single-row Tail summary at submission time; the seed-2024 camera-ready run will extend the training-seed dimension from $n=2$ to $n=3$ without changing the dominant noise source.

Table 20: MUTAG DFS canonical: metrics across training checkpoints (single training seed = 42).

| Step | Precision | Novelty | Unique | ρ | JSD |
|-------|-----------|---------|--------|--------|-------|
| 600 | 0.001 | 0.999 | 0.994 | 0.179 | 0.613 |
| 1200 | 0.031 | 0.969 | 0.859 | 0.550 | 0.214 |
| 2400 | 0.180 | 0.820 | 0.591 | 0.890 | 0.055 |
| 6000 | 0.645 | 0.355 | 0.302 | 0.980 | 0.021 |
| 9600 | 0.768 | 0.232 | 0.231 | 0.993 | 0.021 |
| 12000 | 0.798 | 0.202 | 0.208 | 0.994 | 0.021 |

Table 21: Cross-model comparison: LLM-DFS, LLM-DGMG (both single training seed = 42), DiGress, GraphRNN. Memorization is exact-match graph recall; novelty its complement. GraphRNN is unlabeled and yields no support overlap on larger TU datasets (ρ undefined).

| Dataset | Memorization | | | | Novelty | | | | Spearman ρ | | | | JSD | | | |
|----------|--------------|-------|---------|----------|---------|-------|---------|----------|-----------------|-------|---------|----------|-------|-------|---------|----------|
| | DFS | DGMG | DiGress | GraphRNN | DFS | DGMG | DiGress | GraphRNN | DFS | DGMG | DiGress | GraphRNN | DFS | DGMG | DiGress | GraphRNN |
| MUTAG | 0.828 | 1.000 | 0.000 | 0.000 | 0.172 | 0.000 | 1.000 | 1.000 | 0.983 | 0.990 | 0.621 | 0.063 | 0.030 | 0.013 | 0.217 | 0.554 |
| ENZYMES | 0.975 | 0.989 | 0.000 | 0.000 | 0.025 | 0.011 | 1.000 | 1.000 | 0.939 | 0.944 | 0.777 | – | 0.020 | 0.017 | 0.090 | 0.693 |
| NCI1 | 1.000 | 1.000 | 0.000 | 0.000 | 0.000 | 0.000 | 1.000 | 1.000 | 0.989 | 0.989 | 0.931 | – | 0.015 | 0.018 | 0.038 | 0.693 |
| PROTEINS | 0.891 | 0.918 | 0.005 | 0.000 | 0.109 | 0.082 | 0.995 | 1.000 | 0.980 | 0.985 | 0.761 | – | 0.028 | 0.022 | 0.087 | 0.693 |
| PTC_MR | 0.983 | 0.994 | 0.020 | 0.000 | 0.017 | 0.006 | 0.980 | 1.000 | 0.986 | 0.974 | 0.794 | – | 0.021 | 0.019 | 0.107 | 0.693 |
| PCQM4Mv2 | 0.317 | 0.085 | 0.000 | – | 0.683 | 0.915 | 1.000 | – | 0.976 | 0.945 | 0.247 | – | 0.044 | 0.061 | 0.401 | – |

MUTAG legacy single-decoding aggregate tables. The three tables below retain the original $n=2$ training-seed aggregate (single decoding draw per seed, mean \pm 95% Student- t CI) for historical comparison with earlier drafts. The two-way decoding-seed averaging of Table 24 is the load-bearing report; the wide CIs in the tables below reflect the small training-seed sample size ($t_{0.975}(1) = 12.7$) and the absence of decoding-seed averaging.

Decoding sweep. Table 25 aggregates the six decoding configurations of Table 19 over the available seeds. Spearman ρ stays in 0.94–0.98 across configurations, and precision saturates near 0.99 for every config except `topk_only/pure_sample` (≈ 0.98). The seed-to-seed standard errors on ρ (~ 0.15) are large relative to the across-config spread (~ 0.04), so the single-config readings in the main text should be interpreted with this seed-level uncertainty in mind.

Frequency-stratified metrics. Table 26 reports the seed-aggregated Head/Torso/Tail metrics. The seed-mean Tail- ρ (0.78 ± 0.53 at $n = 2$) is consistent with the seed-42 value (0.82) reported in Table 13: both lie within between-seed variance, and the wide CI is dominated by the small sample size ($t_{0.975}(1) = 12.7$ for $n = 2$). Head and Torso ρ sit near 0.91 and 0.97 with much narrower CI, mirroring the saturation visible in the main-text single-seed results. A definitive seed-stability claim awaits the seed-2024 run currently in progress.

NLL hit/miss analysis. Table 27 aggregates the per-sequence NLL hit/miss test of §6 (Overall distribution alignment) across seeds. The seed-mean Mann–Whitney $p = 0.0753 \pm 0.0113$ does not cross the 0.05 threshold, so on the seeds available we cannot reject the null that hit and miss training sequences carry the same NLL—consistent with the single-seed result and with a memorization-dominated regime in which the model treats reproduced and non-reproduced training sequences alike.

A definitive seed-stability assessment, including the seed=2024 contribution and four-other-TU multi-seed aggregates, is pending completion of the GPU sweep currently underway and will appear in the camera-ready revision.

P PCQM4Mv2: Detailed Results

LLM-DFS memorization summary. Table 28 reports the headline whole-graph numbers behind the main-text PCQM4Mv2 scaling result (§6): precision (exact-match rate) is 0.317, novelty 0.683, and the unique rate saturates at 1.000, so 1024 generations from LLaMA-SMALL produce 1024 distinct DFS codes of which roughly one in three matches a training sequence—the regime in which Spearman ρ stays at 0.98 even though most generations are not verbatim training graphs.

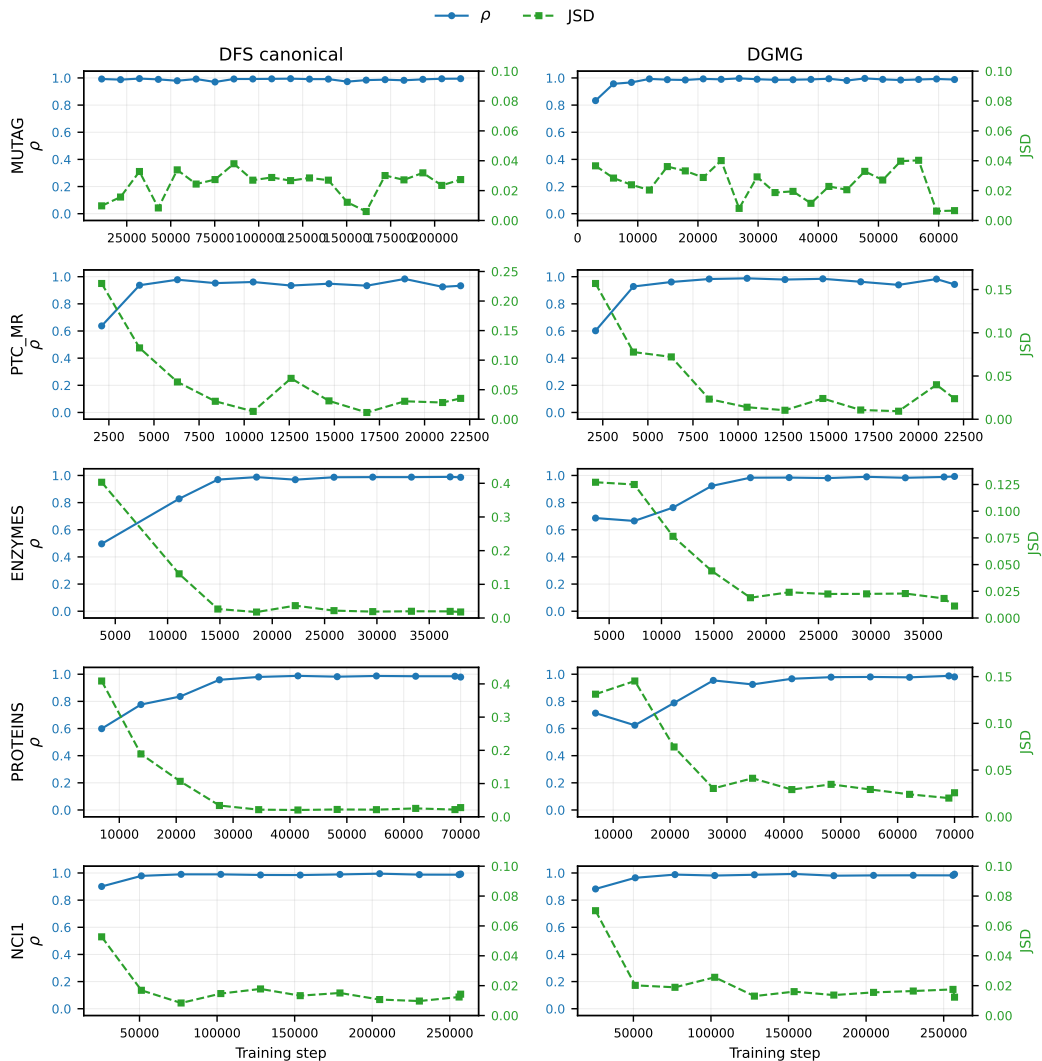


Figure 6: Per-dataset checkpoint trajectories. Rows: TU benchmark datasets. Columns: serialization (DFS canonical / DGMG action sequence). Solid blue: Spearman ρ on the gSpan support intersection (left axis). Dashed green: Jensen–Shannon divergence (right axis, scaled per panel). Precision (memorization rate) trajectories are omitted because the per-checkpoint detector used in the older DGMG runs pre-dates the whole-graph memorization fix described in Appendix H; the corrected end-of-training memorization rates are tabulated in Appendix H, Table 12.

Scaling memorization across training-set sizes. Table 29 contrasts the LLaMA-SMALL exact-match recall and distribution-alignment metrics across the five TU corpora and PCQM4Mv2 under the same architecture and both_default decoding, supporting the headline crossover of the main-text PCQM4Mv2 scaling (§6).

Subsampled evaluation. Table 30 reports gSpan-based metrics averaged over five random 10k-graph training subsamples (against the same 1024 generations) to give a sense of subsample variance. Spearman ρ on the train support is 0.976 ± 0.005 and on the support intersection 0.978 ± 0.005 , with WL-MMD 1.4×10^{-3} and coverage 0.94—tight bands indicating that the $\rho \approx 0.98$ headline of the main-text PCQM4Mv2 scaling (§6) is not an artifact of a single training subsample.

Stratified metrics on PCQM4Mv2 (full). Table 31 reports the full Head/Torso/Tail breakdown for both LLM-DFS and the same-corpus DiGress baseline, extending the Tail-only summary of

Table 22: Appendix: comparison of structural autoregressive baselines on the TU benchmark suite. Memorization, ρ and JSD use the gSpan-based pattern-distribution metrics; structural MMD is computed without label information. DGMG-official is the original implementation by Li et al. (2018) at the published scale ($\sim 100\text{K}$ parameters); LLM-DFS/DGMG numbers (single training seed = 42) are provided for reference in the main paper.

| Dataset | Model | Memorization-based | | gSpan pattern | | | Structural MMD | | |
|----------|---------------|--------------------|---------|---------------|--------|-------|----------------|---------|---------|
| | | Mem. rate | Novelty | Shared | ρ | JSD | WL | deg | orb |
| MUTAG | DiGress | 0.000 | 1.000 | 92 | 0.621 | 0.217 | 0.0780 | 0.00475 | 0.07332 |
| MUTAG | GraphRNN | 0.000 | 1.000 | 16 | 0.063 | 0.554 | 0.2373 | 0.00023 | 0.00011 |
| MUTAG | DGMG-official | 0.000 | 1.000 | 16 | 0.069 | 0.549 | 0.2216 | 0.00108 | 0.00163 |
| PTC_MR | DiGress | 0.020 | 0.980 | 66 | 0.794 | 0.107 | 0.0004 | 0.00225 | 0.00190 |
| PTC_MR | GraphRNN | 0.000 | 1.000 | 0 | n/a | 0.693 | 1.1748 | 0.00010 | 0.00007 |
| PTC_MR | DGMG-official | 0.000 | 1.000 | 0 | n/a | 0.693 | 1.1934 | 0.00011 | 0.00067 |
| ENZYMES | DiGress | 0.000 | 1.000 | 229 | 0.777 | 0.090 | 0.0253 | 0.00228 | 0.00286 |
| ENZYMES | GraphRNN | 0.000 | 1.000 | 0 | n/a | 0.693 | 0.5260 | 0.00004 | 0.00003 |
| ENZYMES | DGMG-official | 0.000 | 1.000 | 0 | n/a | 0.693 | 0.5723 | 0.00876 | 0.00943 |
| PROTEINS | DiGress | 0.005 | 0.995 | 265 | 0.761 | 0.087 | 0.0249 | 0.00075 | 0.00149 |
| PROTEINS | GraphRNN | 0.000 | 1.000 | 0 | n/a | 0.693 | 0.4858 | 0.00003 | 0.00004 |
| PROTEINS | DGMG-official | 0.000 | 1.000 | 0 | n/a | 0.693 | 0.5119 | 0.00142 | 0.00125 |
| NCI1 | DiGress | 0.000 | 1.000 | 317 | 0.931 | 0.038 | 0.0021 | 0.00031 | 0.00305 |
| NCI1 | GraphRNN | 0.000 | 1.000 | 0 | n/a | 0.693 | 1.3392 | 0.00015 | 0.00014 |
| NCI1 | DGMG-official | 0.000 | 1.000 | 0 | n/a | 0.693 | 1.3534 | 0.00143 | 0.00175 |

Table 23: Cross-baseline frequency-stratified diagnostics ($\sigma = 0.1$, upper = 8). LLM-DFS values are mean \pm std over $n = 5$ decoding seeds (Appendix I.4); baselines are single-draw (1024 generated graphs each). DGMG-official and GraphRNN are label-unaware: they emit unlabeled graphs and therefore share essentially no labeled gSpan support with the training set (Head/Torso/Tail miss ≈ 1 , intersection ρ undefined on 4 of 5 datasets); we omit those columns rather than cluttering the table with “1.00/-” rows. “-” indicates ρ_{\cap} is undefined because no patterns are shared in that stratum.

| Dataset | Head miss | | Tail miss | | Tail ρ_{\cap} | |
|----------|-----------|---------|-------------------|---------|--------------------|---------|
| | LLM-DFS | DiGress | LLM-DFS | DiGress | LLM-DFS | DiGress |
| MUTAG | 0.000 | 0.000 | 0.135 \pm 0.099 | 0.719 | 0.420 \pm 0.296 | -0.169 |
| PTC_MR | 0.000 | 0.000 | 0.220 \pm 0.145 | 0.251 | 0.562 \pm 0.456 | -0.157 |
| ENZYMES | 0.000 | 0.000 | 0.132 \pm 0.076 | 0.572 | 0.283 \pm 0.059 | -0.126 |
| PROTEINS | 0.000 | 0.000 | 0.159 \pm 0.056 | 0.471 | 0.258 \pm 0.040 | -0.291 |
| NCI1 | 0.000 | 0.000 | 0.199 \pm 0.075 | 0.613 | 0.350 \pm 0.111 | +0.017 |

Table 3 in the main text. Decoding-stage variance is expected to be substantially smaller on PCQM4Mv2 than on TU: the tail support contains $\sim 10^4$ patterns rather than $\sim 10^2$, so individual sampling noise is absorbed across two orders of magnitude more pattern slots before it can perturb stratum-level summaries (cf. the contrasting large TU std values in Appendix I.4). A full PCQM4Mv2 decoding-seed sweep is left for the camera-ready stage.

Capacity sweep at fixed corpus (DFS canonical, full). Table 32 reports the four-point capacity sweep summarized in Figure 3. Subgraph-level alignment (ρ , JSD) and whole-graph similarity (WL-MMD) stay in narrow bands across the $43\times$ parameter range. Tail rank correlation improves with capacity, reaching its best value at LARGE (Tail $\rho \approx 0.43$); the MEDIUM point (0.34) sits within two standard deviations of TINY and does not break the upward trend. memorization and missing mass instead track tokens-per-parameter: SMALL (128 tok/param) reaches the highest memorization (0.32) and the lowest Tail missing mass (0.07), while the under-trained LARGE (9 tok/param, 12 epochs) memorizes only 0.20 despite $3.4\times$ more parameters. Exact-match recall is therefore bottlenecked by gradient updates rather than parameter budget; the Tail-stratum gains we report for LARGE are likely a lower bound under additional training. We treat this as a diagnostic capacity study rather than a scaling-law fit.

Table 24: Two-way (training-seed \times decoding-seed) ablation on Tail-stratum diagnostics. Each cell is the mean \pm sample std over $n = 5$ decoding seeds (`torch.manual_seed` $\in \{0, 1, 2, 3, 4\}$) at the same training checkpoint. “ ρ_{\cap} ”: intersection Spearman, “ ρ_{tk} ”: trainkeys Spearman (Appendix I.4). Across all 10 cells the decoding-mean shift between training seeds is ≤ 0.05 on Tail miss and ≤ 0.10 on Tail ρ_{\cap} , all within the decoding-seed std. ENZYMES $s_t = 42$ DFS values use the no-cap gBolt rerun (matching Tables 13 and 16); the $s_t = 1337$ ENZYMES DFS column and ENZYMES DGMG rows retain the default cap because the corresponding no-cap multi-seed reruns are deferred to the camera-ready—see Limitations (g).

| Dataset | Mode | Tail miss | | Tail ρ_{\cap} | | Tail ρ_{tk} | |
|----------|------|-------------------|-------------------|--------------------|-------------------|-------------------|-------------------|
| | | $s_t=42$ | $s_t=1337$ | $s_t=42$ | $s_t=1337$ | $s_t=42$ | $s_t=1337$ |
| MUTAG | DFS | 0.135 \pm 0.099 | 0.135 \pm 0.068 | 0.420 \pm 0.296 | 0.402 \pm 0.230 | 0.609 \pm 0.108 | 0.589 \pm 0.093 |
| MUTAG | DGMG | 0.389 \pm 0.181 | 0.472 \pm 0.204 | 0.231 \pm 0.462 | 0.162 \pm 0.540 | 0.457 \pm 0.145 | 0.399 \pm 0.048 |
| PTC_MR | DFS | 0.220 \pm 0.145 | 0.175 \pm 0.096 | 0.562 \pm 0.456 | 0.642 \pm 0.396 | 0.560 \pm 0.418 | 0.596 \pm 0.341 |
| PTC_MR | DGMG | 0.177 \pm 0.119 | 0.196 \pm 0.155 | 0.406 \pm 0.328 | 0.307 \pm 0.436 | 0.412 \pm 0.374 | 0.356 \pm 0.361 |
| ENZYMES | DFS | 0.132 \pm 0.076 | 0.141 \pm 0.086 | 0.283 \pm 0.059 | 0.287 \pm 0.069 | 0.325 \pm 0.049 | 0.329 \pm 0.055 |
| ENZYMES | DGMG | 0.150 \pm 0.105 | 0.170 \pm 0.119 | 0.379 \pm 0.049 | 0.366 \pm 0.056 | 0.430 \pm 0.024 | 0.425 \pm 0.028 |
| PROTEINS | DFS | 0.159 \pm 0.056 | 0.164 \pm 0.065 | 0.258 \pm 0.040 | 0.263 \pm 0.032 | 0.311 \pm 0.038 | 0.316 \pm 0.037 |
| PROTEINS | DGMG | 0.261 \pm 0.102 | 0.288 \pm 0.149 | 0.265 \pm 0.028 | 0.261 \pm 0.047 | 0.321 \pm 0.030 | 0.324 \pm 0.034 |
| NCII | DFS | 0.199 \pm 0.075 | 0.173 \pm 0.060 | 0.350 \pm 0.111 | 0.348 \pm 0.112 | 0.380 \pm 0.094 | 0.376 \pm 0.095 |
| NCII | DGMG | 0.163 \pm 0.093 | 0.184 \pm 0.082 | 0.296 \pm 0.031 | 0.278 \pm 0.092 | 0.310 \pm 0.044 | 0.282 \pm 0.042 |

Table 25: MUTAG, DFS canonical, multi-seed aggregate (2 seeds: {42, 1337}; seed 2024 in progress, see Sec. A; mean \pm SE).

| Config | Unique | Precision | Novelty | ρ | JSD | Missing |
|--------------|---------------------|-----------------------|-----------------------|---------------------|---------------------|---------------------|
| both_default | 0.1636 \pm 0.0062 | 1.0000 | 0.0000 | 0.9829 \pm 0.0282 | 0.0298 \pm 0.0021 | 0.0193 \pm 0.2157 |
| nucleus_only | 0.1641 | 1.0000 | 0.0000 | 0.9856 \pm 0.0558 | 0.0171 \pm 0.0139 | 0.0211 \pm 0.2678 |
| topk_only | 0.1851 \pm 0.0062 | 0.9894 \pm 3.54e-04 | 0.0106 \pm 3.54e-04 | 0.9913 \pm 0.0057 | 0.0224 \pm 0.0162 | 0.0424 \pm 0.0507 |
| pure_sample | 0.1860 \pm 0.0310 | 0.9817 \pm 0.0970 | 0.0183 \pm 0.0970 | 0.9940 \pm 0.0445 | 0.0174 \pm 0.0452 | 0.0378 \pm 0.0187 |
| tp_high | 0.1816 | 1.0000 | 0.0000 | 0.9792 \pm 0.0290 | 0.0371 \pm 0.0355 | 0.0788 \pm 0.0432 |
| tp_low | 0.1201 | 1.0000 | 0.0000 | 0.9573 \pm 0.1300 | 0.0511 \pm 0.0360 | 0.0178 \pm 0.0298 |

Checkpoint trajectory. Figure 8 traces unique-rate, precision, and Spearman ρ across PCQM4Mv2 training for the four LLaMA capacities. Unlike the small-corpus MUTAG dynamics (Figure 9), unique rate stays at 1.0 throughout training and precision climbs only mildly with steps while increasing with capacity at fixed step budget—i.e. at this scale the model never collapses onto the training corpus, and larger capacity buys a larger memorized fraction rather than faster memorization.

DGMG capacity sweep. A three-point sweep on DGMG (identical 20-epoch schedule for all three sizes) reproduces the DFS pattern and additionally separates two regimes. Subgraph-level alignment (ρ , JSD) and whole-graph similarity (WL-MMD) improve sharply from TINY (4.2M) to MEDIUM (85M) (ρ : 0.89 \rightarrow 0.95, JSD: 0.29 \rightarrow 0.25, WL-MMD: 0.0037 \rightarrow 0.0021) and saturate between MEDIUM and SMALL (113M; ρ shifts by < 0.005 , WL-MMD by 10%). Missing-mass metrics keep improving across all three sizes: Tail missing mass drops 0.56 \rightarrow 0.20 \rightarrow 0.13 (76% overall) and train missing mass drops 0.09 \rightarrow 0.02 \rightarrow 0.02. memorization scales monotonically with capacity (0.007 \rightarrow 0.060 \rightarrow 0.085), mirroring the DFS pattern when training duration is held constant. Because all three DGMG variants share the schedule, the capacity effect is uncontaminated by duration differences and provides a cleaner read on the scaling dimension that the DFS sweep partially confounds with training length. The headline trends—monotonic capacity gains on rank correlation; diminishing returns on distributional alignment beyond ~ 100 M parameters—generalize across the two serializations.

Extended capacity check (DGMG-large). We add a fourth, larger point at LARGE (419.7M parameters), trained for 12 epochs under a fixed compute budget so its tokens-per-parameter ratio (5.8) sits well below the other three sizes (960, 47.9, 35.9 for TINY/MEDIUM/SMALL). Despite this under-training, LARGE matches or exceeds all three smaller variants on every subgraph-level alignment metric ($\rho = 0.964$, JSD = 0.052) and whole-graph similarity (WL-MMD = 0.0020), continues the monotonic Tail ρ improvement (0.158 \rightarrow 0.241 \rightarrow 0.246 \rightarrow 0.279), and pushes Tail

Table 26: MUTAG, DFS canonical, multi-seed strata aggregate (2 seeds: {42, 1337}; seed 2024 in progress; mean \pm 95% Student-*t* CI).

| Stratum | Shared | Train-only | Missing | ρ | JSD |
|---------|------------------------|------------------------|---------------------|---------------------|-------------------------|
| head | 70.0000 | 0.0000 | 0.0000 | 0.9112 | $4.67e-05 \pm 5.59e-04$ |
| torso | 440.0000 | 0.0000 | 0.0000 | 0.9719 ± 0.0407 | $8.39e-04 \pm 0.0050$ |
| tail | 91.0000 ± 368.4799 | 33.0000 ± 368.4799 | 0.2664 ± 2.9815 | 0.7788 ± 0.5289 | 0.1138 ± 1.3038 |

Table 27: MUTAG, DFS canonical, multi-seed NLL analysis (2 seeds: {42, 1337}; seed 2024 in progress).

| Group | n | Mean NLL | Median NLL |
|------------------------------------|-------------|---------------------|---------------------|
| Hit | 168 ± 6 | 0.4762 ± 0.6322 | 0.3506 ± 0.3347 |
| Miss | 20 ± 6 | 0.5899 ± 1.0248 | 0.4814 ± 1.0688 |
| MW p -value: 0.0564 ± 0.2458 | | | |

missing mass to its lowest value (0.093, vs. 0.132 at SMALL). memorization also keeps rising with capacity ($0.085 \rightarrow 0.115$) even at 5.8 tokens per parameter, indicating that the head of the distribution is recoverable with a fraction of the optimal training budget. The four-point sweep therefore preserves both the saturation of subgraph-level alignment and whole-graph similarity around 100M parameters and the monotonic Tail-stratum gains with capacity that we observe in the DFS sweep (Table 32).

Novel-only subset analysis. A natural concern is that the high ρ on PCQM4Mv2 might still be driven by the non-trivial memorized fraction. To test this directly, we recompute gSpan on the novel-only subset $\mathbf{D}_{\text{gen}} \setminus \mathbf{D}_{\text{tr}}$ (679, 730, 797 graphs out of 1024 for SMALL/MEDIUM/LARGE, novelty 66–78%) against a fixed 10,000-graph training subsample with the same gSpan settings ($\sigma = 0.1$, upper = 8). Table 34 shows that the novel-only Spearman ρ tracks the all-generation reference within 0.026 at every capacity (per-row gaps: SMALL 0.004, MEDIUM 0.026, LARGE 0.014), even though the novel subset by construction excludes the memorized graphs. The distributional alignment is therefore not driven solely by the memorized fraction.

DiGress comparator. Tables 35–37 report the DiGress baseline at PCQM4Mv2 scale under the same diagnostic. DiGress occupies the opposite corner of the memorization–alignment plane to the LLM: precision is 0.000 (no exact-match recall over 200 generated graphs) and distributional alignment collapses (Spearman on the train support 0.247 ± 0.051 , train missing mass 0.699 ± 0.031 , JSD 0.401 ± 0.031), with the Tail stratum showing the same pattern. The contrast positions the LLM regime as *distinct* from low-memorization diffusion—high ρ with moderate memorization rather than low ρ with near-zero memorization.

Q Learning Dynamics

Figure 9 shows the evolution of key metrics across training checkpoints.

A consistent three-phase pattern emerges across the five TU datasets (see Figure 6 for the per-dataset trajectories): (1) a *random generation phase* early in training ($\rho < 0.5$, precision $\approx 0\%$, novelty $\approx 100\%$); (2) a *rapid memorization phase* where ρ rises sharply from ~ 0.5 to > 0.9 in lockstep with precision; and (3) a *saturation phase* ($\rho > 0.94$, precision 80–100%) in which further training yields marginal improvement. Critically, the rise in ρ is *synchronized* with the rise in memorization rate, not delayed. The MUTAG DFS trajectory illustrates this: at step 600, precision is 0.1% and $\rho = 0.18$; by step 2400, precision reaches 18% and $\rho = 0.89$; at the final checkpoint (step ~ 12000), precision is 79.8% and $\rho = 0.99$.

Table 28: PCQM4Mv2 LLM-DFS memorization summary (single training seed = 42; 3,104,677 unique training DFS sequences out of 3,371,958 total; 1024 generated samples).

| Metric | Value |
|--------------|--------------|
| Train total | 3371958 |
| Train unique | 3104677 |
| Gen total | 1024 |
| Gen unique | 1024 |
| Unique rate | 1.0000 |
| Precision | 0.3174 |
| Novelty | 0.6826 |
| Recall | $1.05e - 04$ |

Table 29: Scaling memorization across training-set sizes (DFS canonical, both_default). At PCQM4Mv2 scale, memorization drops from $\sim 100\%$ to 31.7% with the *same* 132M-parameter LLaMA-SMALL architecture and token budget shape, while Spearman ρ remains high.

| Dataset | #Graphs | Memorization | Novelty | Unique | ρ | JSD |
|----------|---------|--------------|---------|--------|--------|-------|
| MUTAG | 188 | 0.828 | 0.172 | 0.199 | 0.976 | 0.035 |
| PTC_MR | 344 | 0.983 | 0.017 | 0.285 | 0.950 | 0.063 |
| ENZYMES | 600 | 0.975 | 0.025 | 0.430 | 0.939 | 0.019 |
| PROTEINS | 1113 | 0.891 | 0.109 | 0.591 | 0.988 | 0.022 |
| NCI1 | 4110 | 1.000 | 0.000 | 0.862 | 0.990 | 0.010 |
| PCQM4Mv2 | 3746620 | 0.317 | 0.683 | 1.000 | 0.976 | 0.044 |

Table 30: PCQM4Mv2 LLM-DFS subsample evaluation (single training seed = 42; 5 random subsamples for reference-side variance estimation only, not training- or decoding-seed variance).

| Metric | mean \pm std |
|-------------------------------|-------------------------|
| Shared patterns | 252.0 ± 3.8 |
| Train-only patterns | 3.2 ± 0.4 |
| Test-only patterns | 75.0 ± 3.8 |
| Train mass missing | 0.0065 ± 0.0008 |
| Test mass novel | 0.1153 ± 0.0062 |
| JS divergence | 0.0444 ± 0.0023 |
| Spearman (ρ on train) | 0.9758 ± 0.0049 |
| Spearman (ρ on \cap) | 0.9779 ± 0.0050 |
| WL MMD | $0.0014 \pm 1.96e - 04$ |
| WL coverage | 0.9400 ± 0.0030 |

Table 31: Stratified metrics on PCQM4Mv2 (single training seed = 42; mean \pm std over 5 random 10k training-reference subsamples; reference-side variance only, not training- or decoding-seed variance; c.f. caption of Table 3). LLM-DFS reproduces Head/Torso almost perfectly and only loses ground in the Tail; DiGress collapses uniformly with Head missing-mass already at 46.5%. The contrast separates “high ρ with non-trivial memorization” (LLM-DFS) from “low ρ with weak labeled-substructure alignment” (DiGress).

| Model | Stratum | Missing | JSD | ρ |
|---------|---------|---------------------|---|---------------------|
| LLM-DFS | Head | 0.0000 ± 0.0000 | $3.07 \times 10^{-4} \pm 4.65 \times 10^{-5}$ | 0.9834 ± 0.0043 |
| | Torso | 0.0045 ± 0.0015 | $0.0022 \pm 5.28 \times 10^{-4}$ | 0.9630 ± 0.0087 |
| | Tail | 0.0694 ± 0.0170 | 0.0255 ± 0.0062 | 0.4061 ± 0.2223 |
| DiGress | Head | 0.4650 ± 0.0527 | 0.2007 ± 0.0280 | 0.5385 ± 0.0330 |
| | Torso | 0.7765 ± 0.0331 | 0.4117 ± 0.0290 | 0.1395 ± 0.0333 |
| | Tail | 0.8600 ± 0.0328 | 0.4887 ± 0.0288 | 0.0463 ± 0.2115 |

Table 32: Model-size scaling on PCQM4Mv2 (DFS canonical, both_default, single training seed = 42; mean \pm half-width over 5 random 10 k-graph training-reference subsamples for a single 1024-graph generation; reference-side variance only, not training- or decoding-seed variance; c.f. caption of Table 3; memorization on the full 3.37M unique training set). Tok/Param = total training tokens divided by parameter count; TINY/MEDIUM/SMALL are trained for 50 epochs and LARGE for 12 epochs (compute budget).

| Model | Params | Tok/Param | Memorization | ρ | Tail ρ | Tail miss | WL-MMD |
|--------------|---------|----------------|--------------|--------|-------------|-----------|--------|
| LLaMA-tiny | 10.5 M | 1600 | 0.126 | 0.9644 | 0.3740 | 0.1768 | 0.0023 |
| LLaMA-medium | 99.1 M | 170 | 0.258 | 0.9482 | 0.3355 | 0.1915 | 0.0016 |
| LLaMA-small | 132.2 M | 128 | 0.317 | 0.9758 | 0.4061 | 0.0694 | 0.0014 |
| LLaMA-large | 451.0 M | 9 [†] | 0.198 | 0.9686 | 0.4286 | 0.1614 | 0.0023 |

[†] Chinchilla-suboptimal: trained for 12 epochs (\sim 4B tokens) due to compute budget.

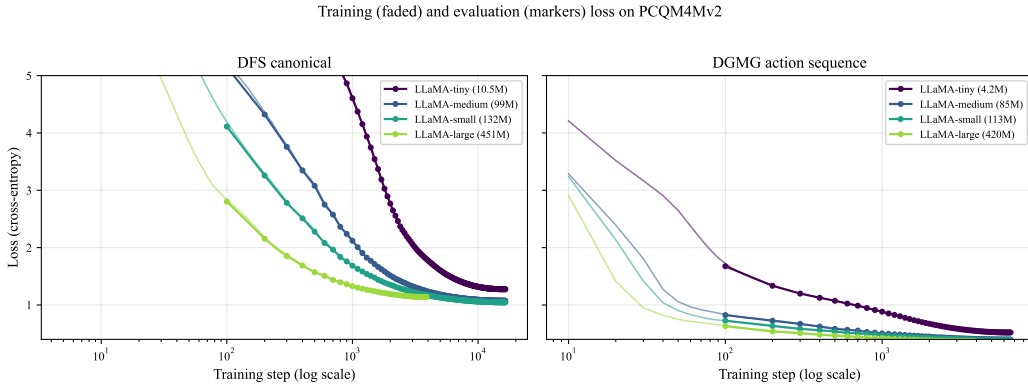


Figure 7: Training (faded curves) and held-out evaluation (markers) cross-entropy loss on PCQM4Mv2 across model sizes; training step on a log axis to match Figure 8. Left: DFS canonical (TINY/MEDIUM/SMALL share a 50-epoch schedule, LARGE a 12-epoch schedule). Right: DGMG action sequence (TINY/MEDIUM/SMALL share a 20-epoch schedule, LARGE a 12-epoch schedule). Loss separation by capacity is consistent across both serializations: larger models reach lower train and eval loss in every regime we examine.

PCQM4Mv2 LLM-DFS checkpoint trajectory across model capacities

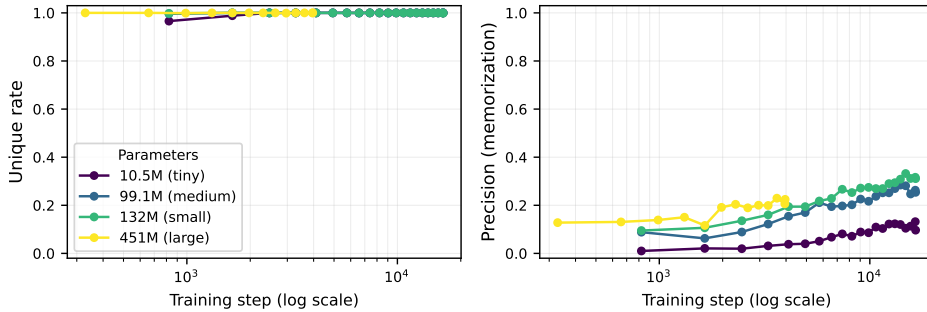


Figure 8: PCQM4Mv2 LLM-DFS checkpoint trajectory across the four LLaMA capacities sweep (10.5M, 99.1M, 132M, 451M parameters; legend ordered by parameter count, not by the upstream TINY/MEDIUM/SMALL/LARGE naming which is non-monotonic in size). Training step on a log axis. Unique rate saturates at 1.0 within the first 10^3 steps and stays there for every capacity, while precision (memorization) rises only mildly with training and increases with capacity at fixed step budget—in sharp contrast to the small-corpus MUTAG dynamics in Figure 9, where precision climbs to 0.8 over the same step range.

Table 33: Model-size scaling on PCQM4Mv2 (DGMG action sequences, single training seed = 42; 20-epoch schedule for TINY/MEDIUM/SMALL, 12-epoch budget-limited schedule for LARGE, marked †; mean \pm half-width over 5 random 10k-graph reference subsamples; reference-side variance only, not training- or decoding-seed variance; memorization on the full 3.10M unique training DFS sequences). Parameter counts are smaller than the DFS counterparts because the DGMG vocabulary is ~ 86 tokens versus 12,297 for DFS.

| Model | Params | Memorization | ρ | Tail ρ | Tail miss | WL-MMD |
|--------------|---------|--------------|--------|-------------|-----------|--------|
| LLaMA-tiny | 4.2 M | 0.007 | 0.8890 | 0.1579 | 0.5555 | 0.0037 |
| LLaMA-medium | 85.1 M | 0.060 | 0.9481 | 0.2412 | 0.2009 | 0.0021 |
| LLaMA-small | 113.4 M | 0.085 | 0.9452 | 0.2457 | 0.1317 | 0.0023 |
| LLaMA-large† | 419.7 M | 0.115 | 0.9635 | 0.2790 | 0.0928 | 0.0020 |

† Trained for 12 epochs (~ 2.4 B tokens, 5.8 tokens/parameter) vs. 20 epochs (~ 4.1 B tokens) for the other three sizes.

Table 34: PCQM4Mv2 novel-only gSpan against a fixed 10,000-graph training subsample ($\sigma = 0.1$, upper = 8; single training seed = 42, single 1024-graph generation draw). “All-gen ρ ” is the Spearman on the full 1024-graph generation, computed under the same single-subsample reference for fair comparison and therefore differs from the 5-subsample averages in Tables 29–3; the salient quantity is the small all-vs-novel gap.

| Size | n_{gen} | Novelty | All-gen ρ | Novel-only subset | | |
|--------|------------------|---------|----------------|-------------------|-------|-------|
| | | | | ρ | JSD | MM |
| SMALL | 1024 | 0.663 | 0.793 | 0.789 | 0.136 | 0.130 |
| MEDIUM | 1024 | 0.713 | 0.798 | 0.824 | 0.144 | 0.147 |
| LARGE | 1024 | 0.778 | 0.822 | 0.808 | 0.146 | 0.134 |

Table 35: PCQM4Mv2 DiGress memorization summary (DiGress open-source checkpoint; comparison LLM numbers use single training seed = 42).

| Metric | Value |
|--------------|---------|
| Train total | 3371958 |
| Train unique | 3104677 |
| Gen total | 200 |
| Gen unique | 200 |
| Unique rate | 1.0000 |
| Precision | 0.0000 |
| Novelty | 1.0000 |
| Recall | 0.0000 |

Table 36: PCQM4Mv2 DiGress subsample evaluation (5 random reference subsamples, reference-side variance only).

| Metric | mean \pm std |
|-------------------------------|---------------------|
| Shared patterns | 58.2 \pm 8.1 |
| Train-only patterns | 197.0 \pm 6.4 |
| Test-only patterns | 72.8 \pm 8.1 |
| Train mass missing | 0.6988 \pm 0.0308 |
| Test mass novel | 0.3326 \pm 0.0605 |
| JS divergence | 0.4006 \pm 0.0307 |
| Spearman (ρ on train) | 0.2473 \pm 0.0512 |
| Spearman (ρ on \cap) | 0.7008 \pm 0.0658 |
| WL MMD | 0.0237 \pm 0.0146 |
| WL coverage | 0.9034 \pm 0.0194 |

Table 37: PCQM4Mv2 DiGress strata (5 random reference subsamples, reference-side variance only).

| Stratum | Missing | JSD | ρ |
|---------|---------------------|---------------------|---------------------|
| Head | 0.4650 ± 0.0527 | 0.2007 ± 0.0280 | 0.5385 ± 0.0330 |
| Torso | 0.7765 ± 0.0331 | 0.4117 ± 0.0290 | 0.1395 ± 0.0333 |
| Tail | 0.8600 ± 0.0328 | 0.4887 ± 0.0288 | 0.0463 ± 0.2115 |

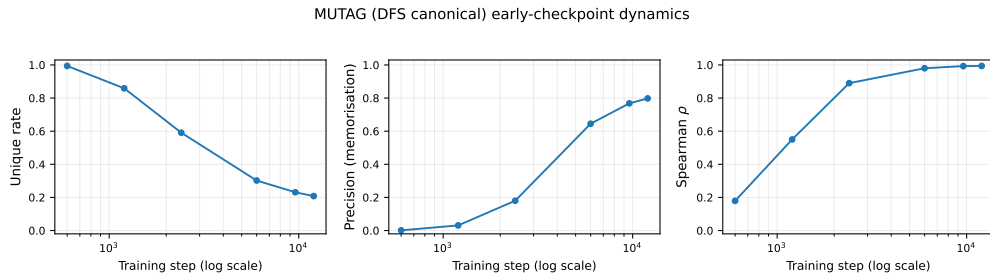


Figure 9: MUTAG (DFS canonical) early-checkpoint dynamics. Unique rate, precision, and Spearman ρ are tracked across training checkpoints. Spearman ρ rises in lockstep with precision, indicating that distributional alignment is acquired *simultaneously* with memorization rather than after it. Per-dataset checkpoint trajectories for the remaining four TU datasets are reported in Figure 6.